

Fig. III-11.

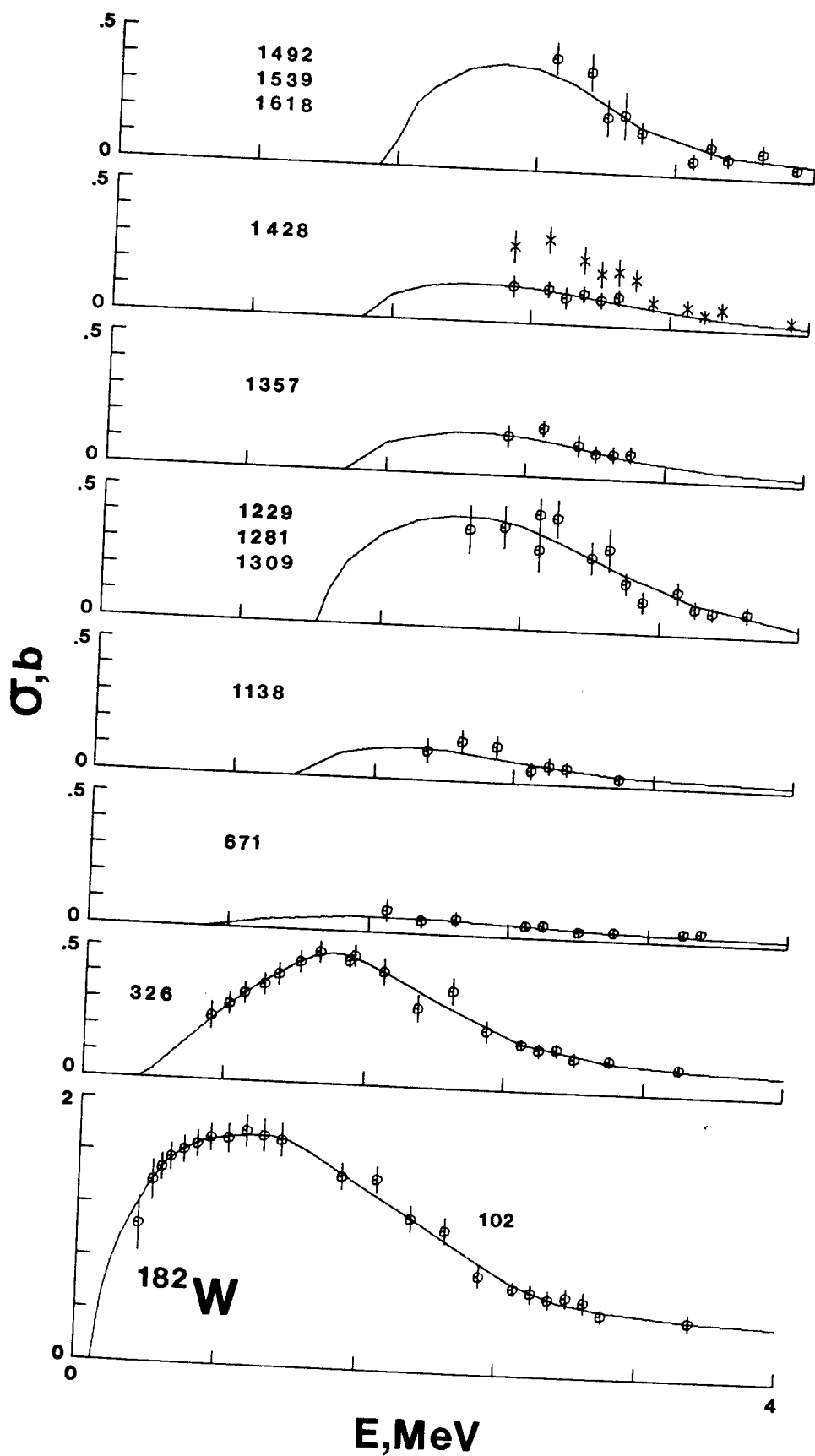


Fig. III-12A.

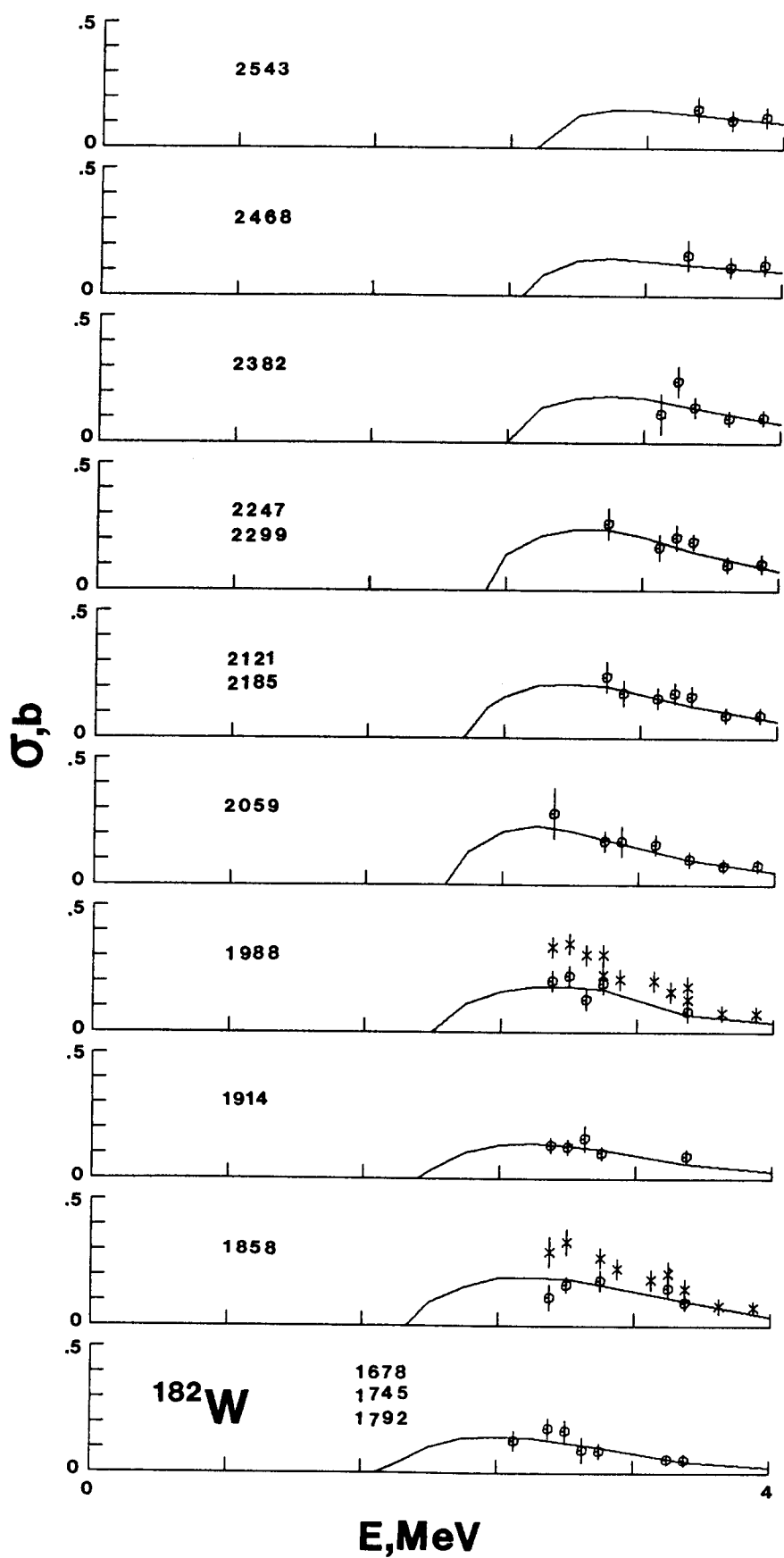


Fig. III-12A (Contd.)

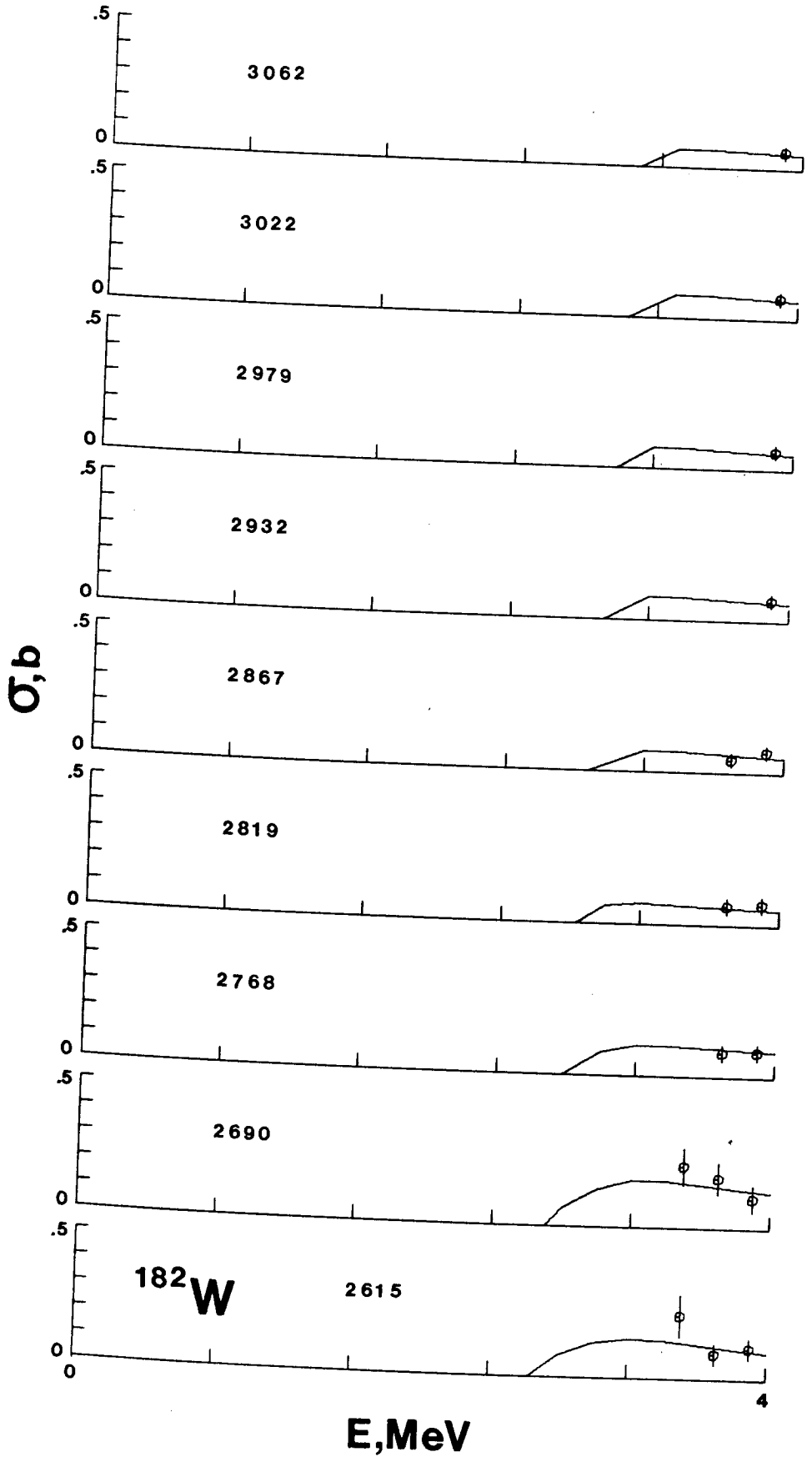


Fig. III-12A (Contd.)

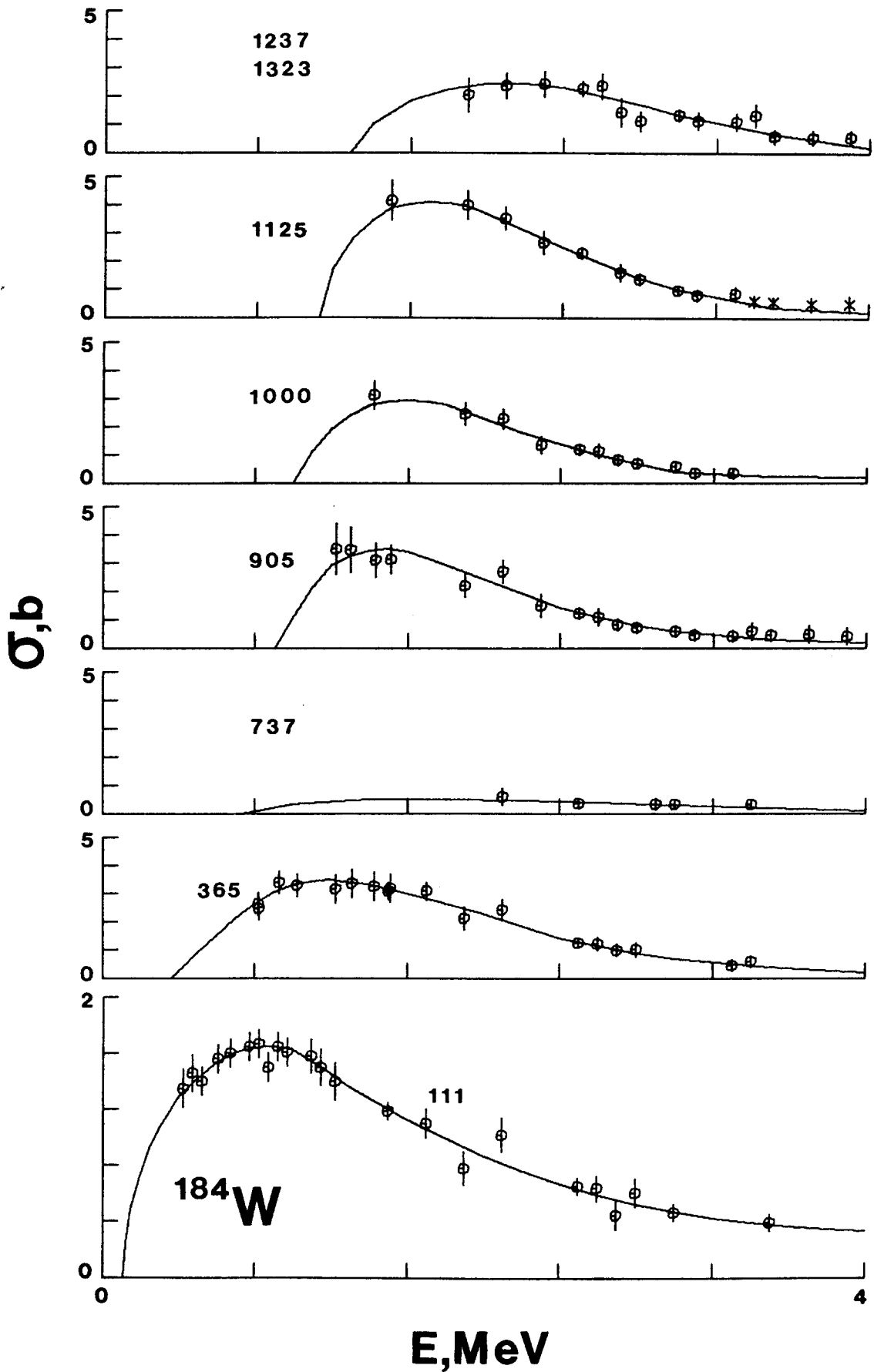


Fig. III-12B.

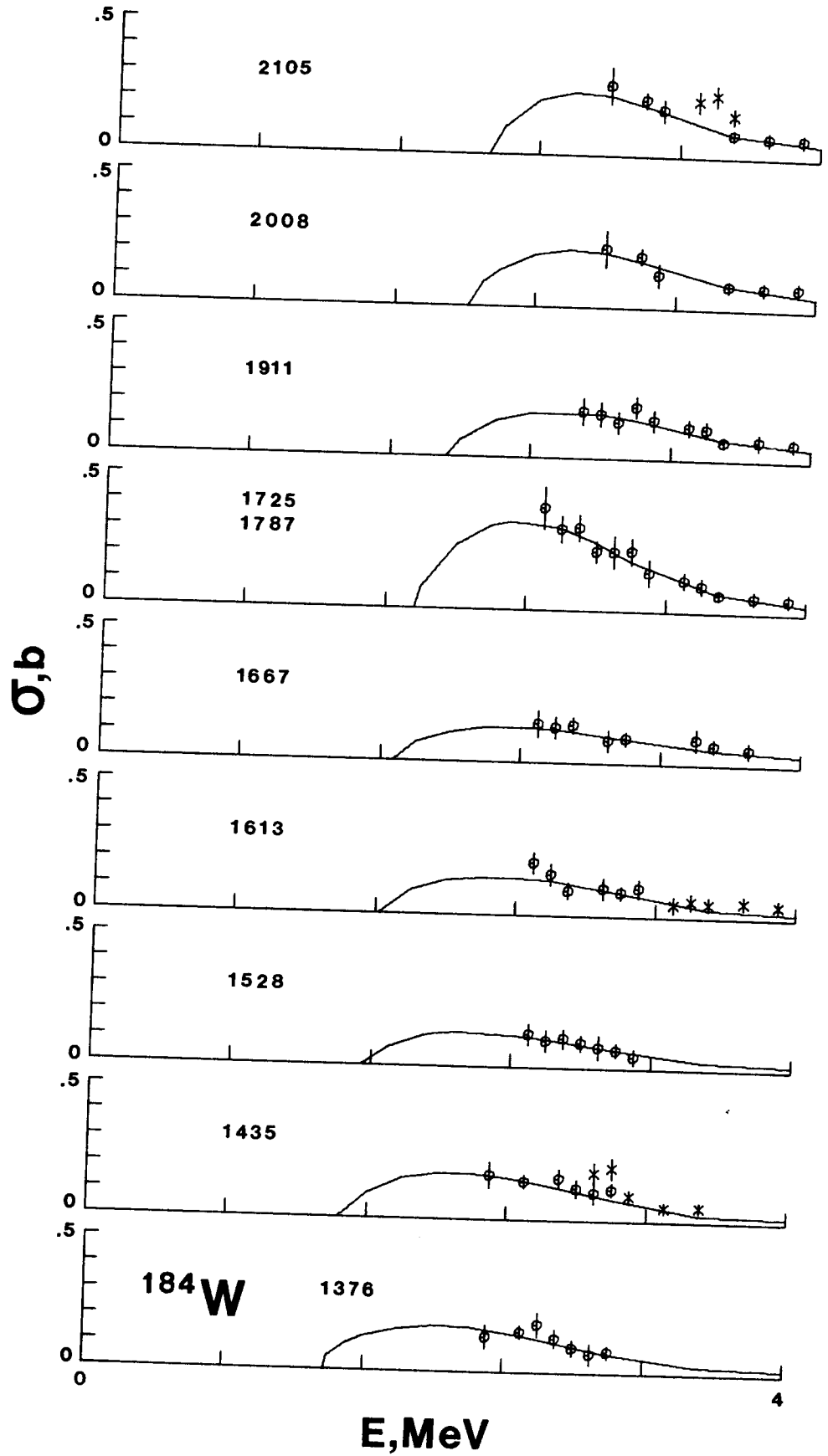


Fig. III-12B (Contd.).

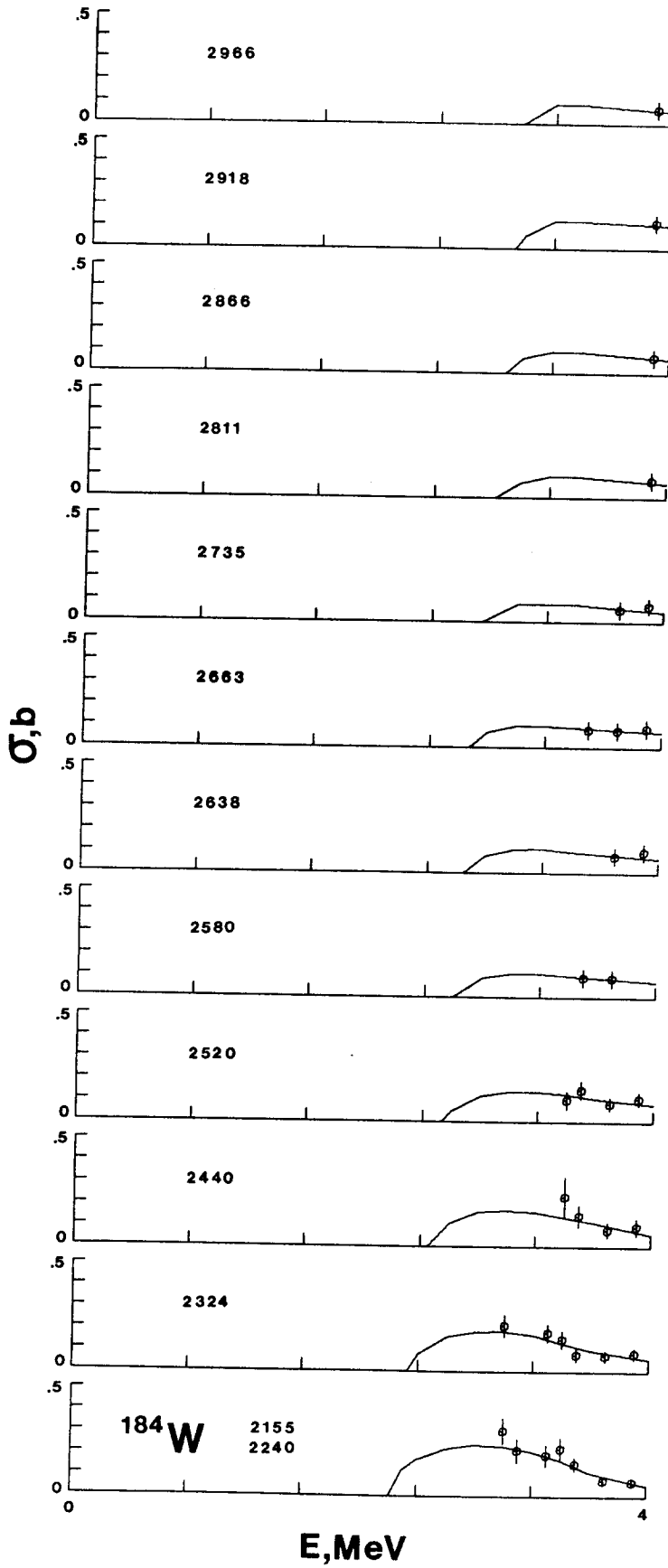


Fig. III-12B (Contd.).

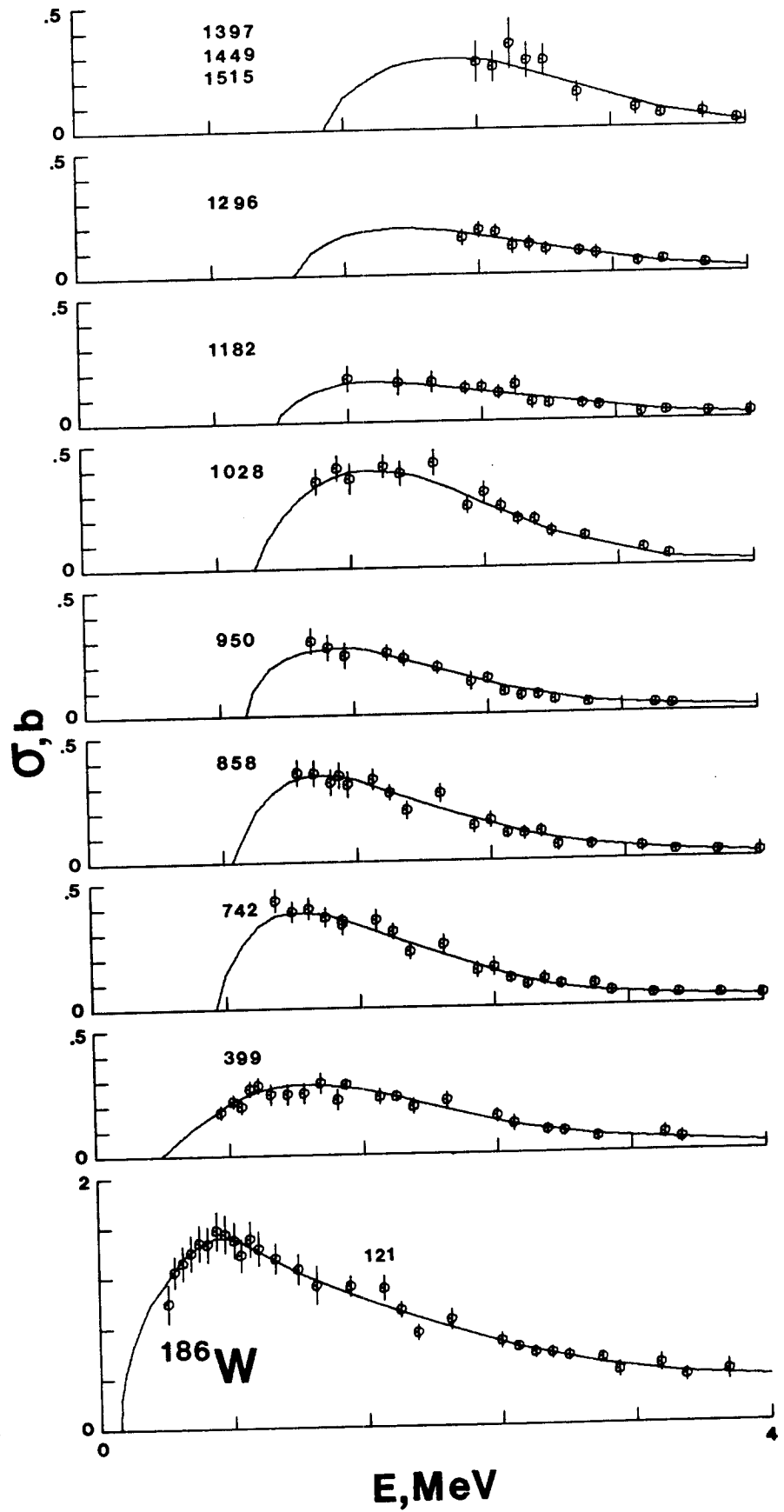


Fig. III-12C.

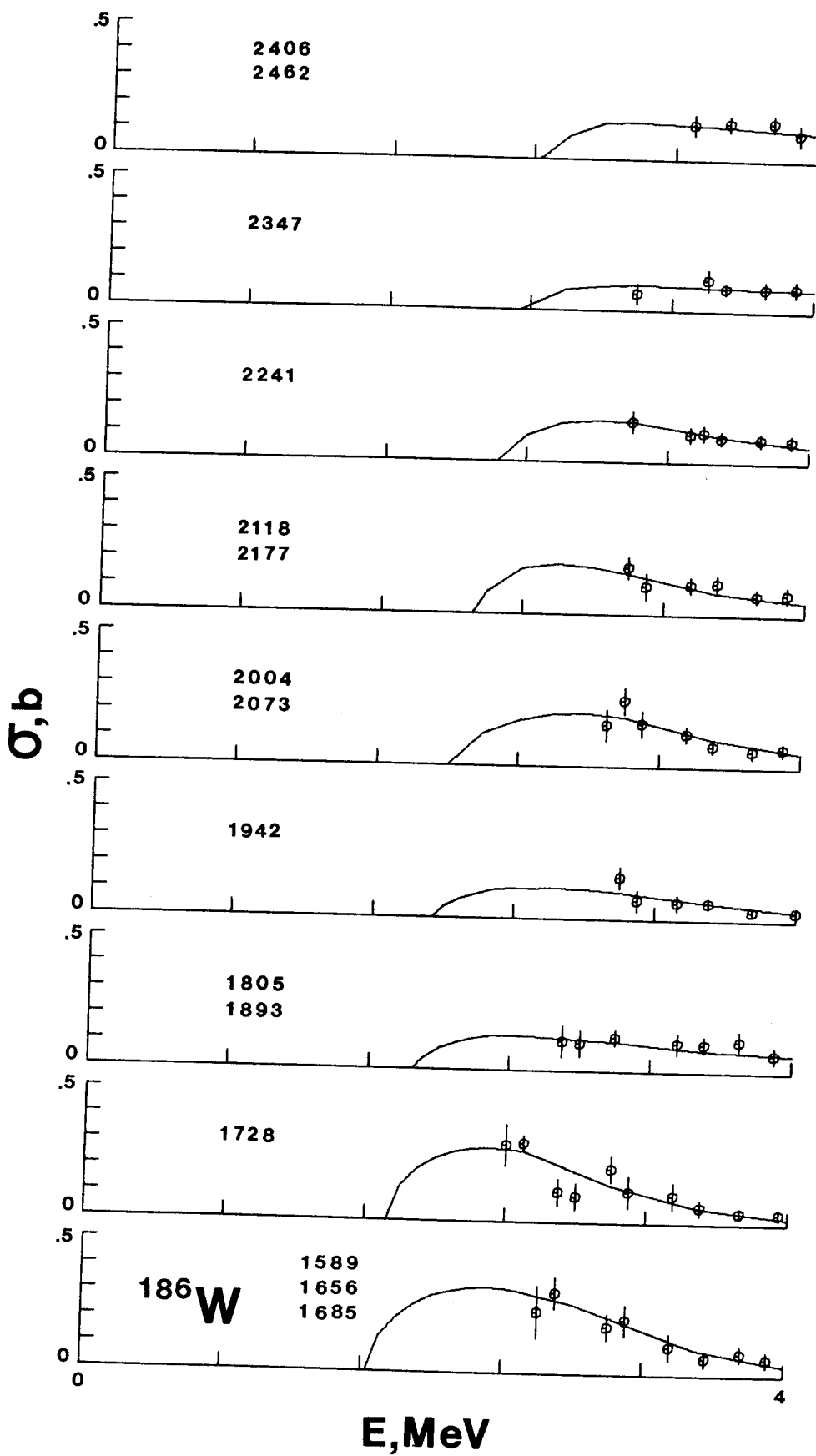


Fig. III-12C (Contd.).

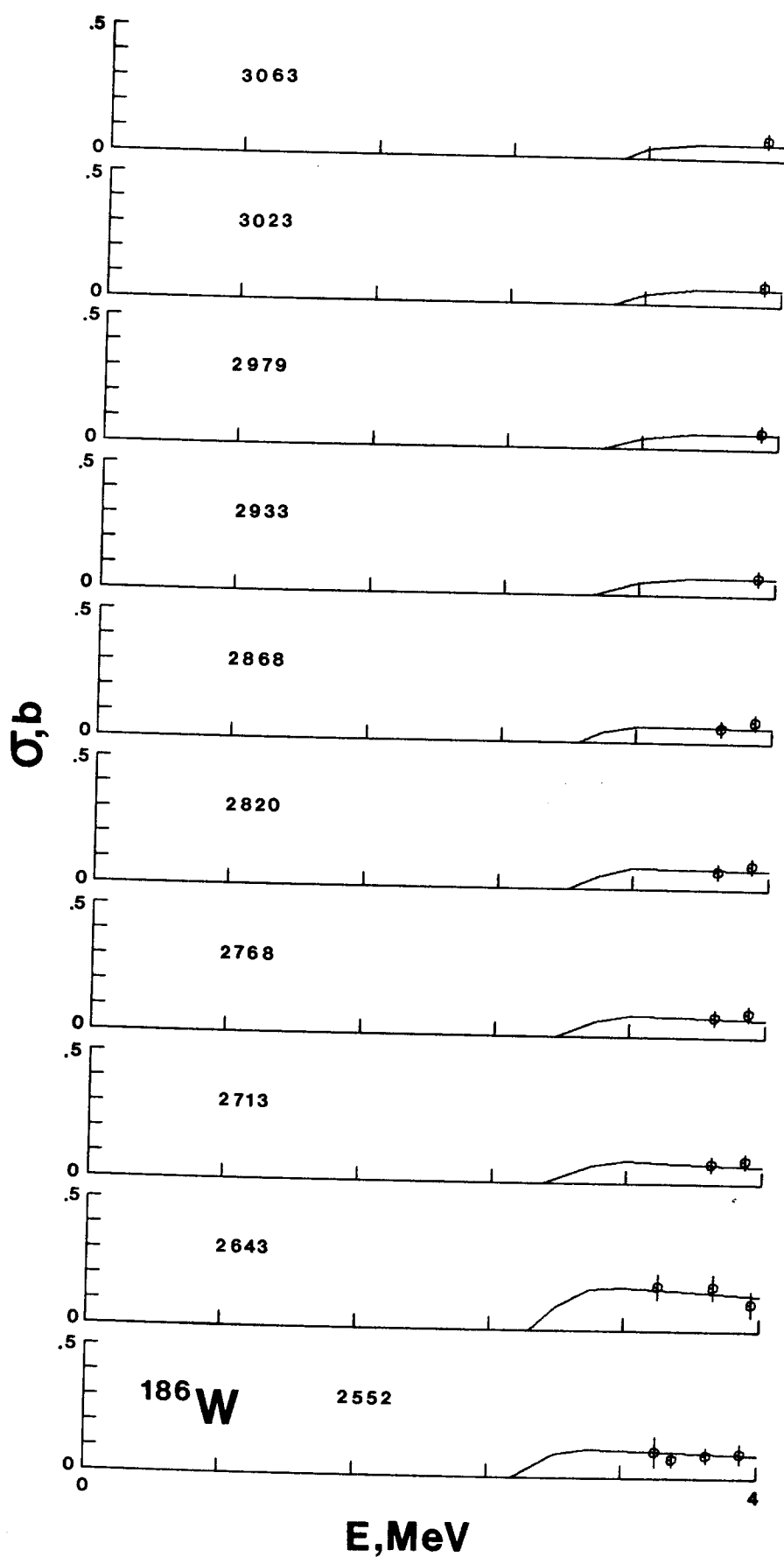


Fig. III-12C (Contd.).

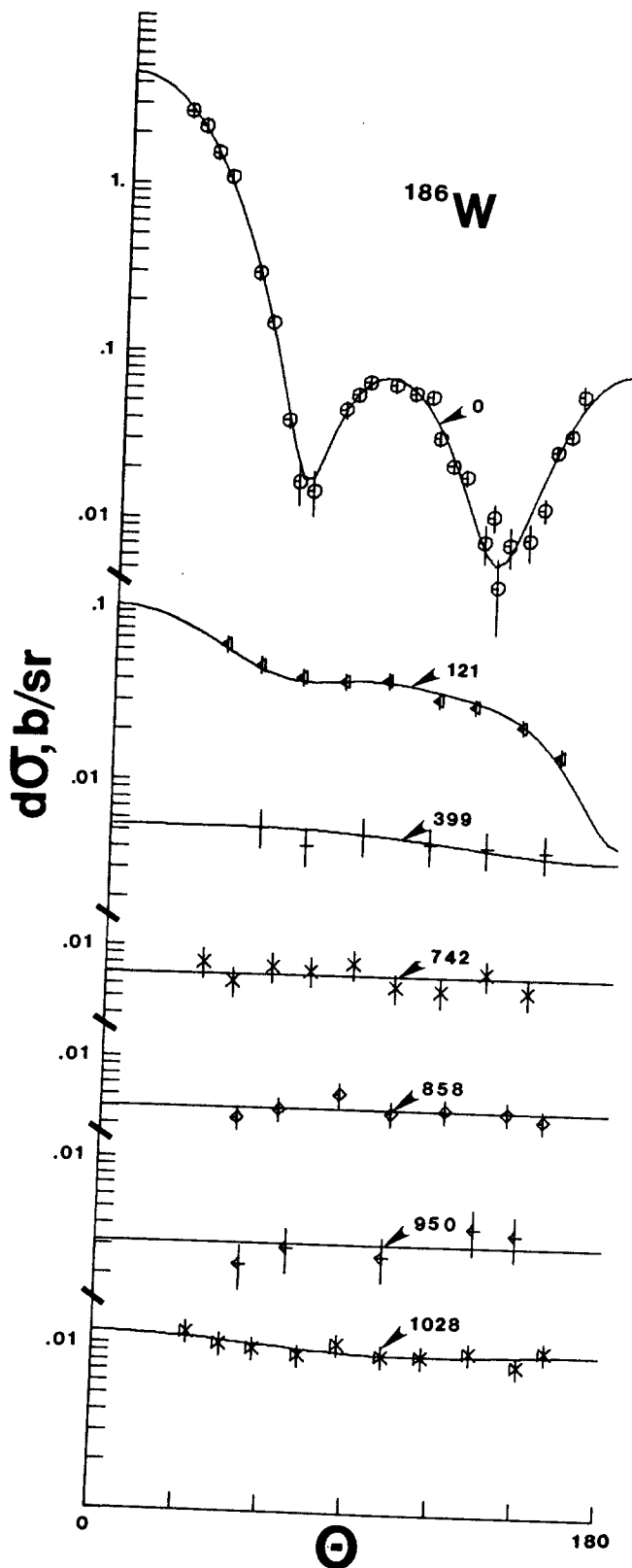


Fig. III-13.

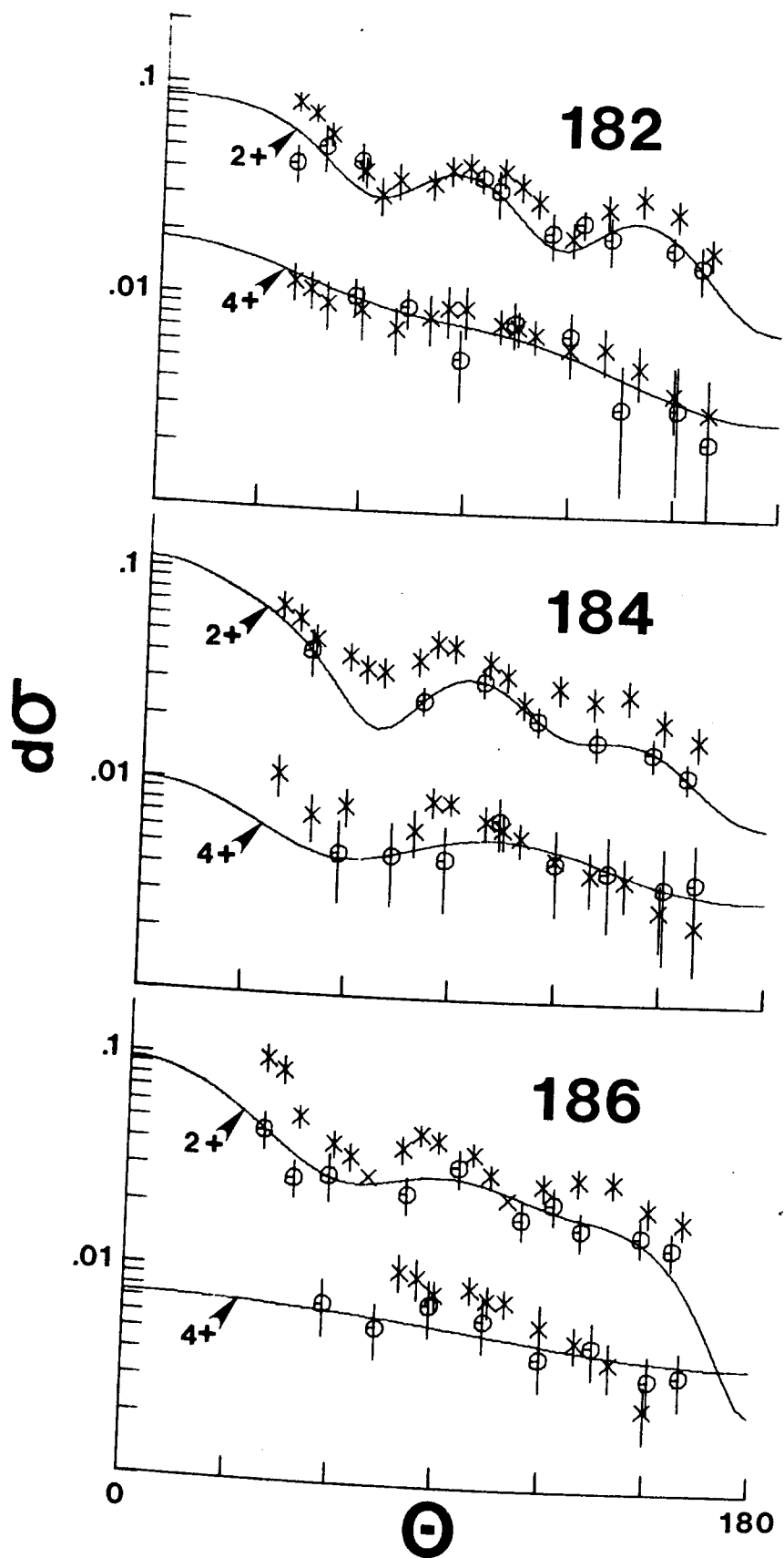


Fig. III-14.

#### IV. PHYSICAL INTERPRETATION

The objective was a "base" physical model descriptive of the present experimental results and suitable for a subsequent investigation of some of the physical aspects of the measured quantities in the context of that model. The interpretation was based upon the coupled-channels model (IV-1). The neutron cross sections were calculated using the computational code JUSTSO (IV-2). This code treats the direct reactions in the coupled-channels formalism. It also determines the transmission coefficients from the deformed potential and calculates the compound-nucleus contributions using the Hauser-Feshbach formula with resonance width-fluctuation and correlation corrections (IV-3). The latter correction factors were calculated using the formalism of Moldauer (IV-4) which gives consideration to the enhancement of both elastic- and inelastic-neutron processes in the coupled-channels. The calculations explicitly included the inelastic-neutron excitation of levels to ~1.5 MeV using the energetics, spins and parities of Ref. IV-5. Compound-nucleus competition due to higher-energy levels was approximated using the statistical level-density parameters of Gilbert and Cameron (IV-6). Radiative-capture processes were neglected, an omission that had negligible effect in the context of the present experiments.

The "base" model employed the potential of Delaroche et al. (IV-7), the parameters of which are summarized in Table IV-1. That potential will be shown to be generally descriptive of the present experimental results and it is supported by extensive parameter studies by one of the present authors reported elsewhere (IV-8). In comparing calculations with measured values, the present experimental results were used, extended to lower energies with experimental values previously reported from this laboratory (IV-9). The experimental and calculational comparison followed a hierarchy. First attention was given to neutron total cross sections. They were most accurately measured and are unambiguously calculable. Next, the comparisons gave attention to angle-integrated partial cross sections associated with the ground-state rotational band; i.e. elastic scattering and the inelastic excitation of the first 2+ and 4+ states. These angle-integrated cross sections were well defined by the experiments and easily calculable at low energies where the compound-nucleus contribution can be reasonably determined, and at high energies where the cross sections are essentially due to direct processes. Comparisons of measured and calculated angle-differential cross sections of the ground-state rotational band were considered; however, some such comparisons deal with very small and experimentally uncertain magnitudes. The neutron-excitation of higher-lying levels was calculated using an equivalent spherical potential, but the results were not directly used in judgments of model validity as the contributing structure remained uncertain in many cases, both from the points of view of measurement and calculation. No attention was given to low-energy strength functions as they are experimentally uncertain and their remain questions as to their interpretation (IV-10).

The measured neutron total cross sections are compared with those calculated from the "base" model in Fig. IV-1. The  $^{184}\text{W}$  and  $^{186}\text{W}$  results agree to within several percent over the full measured energy range (0.1-5.0 MeV). The agreement is less satisfactory for  $^{182}\text{W}$  where the calculated results tend to be higher than the measured values below 1.0 MeV. At low energies the

self-shielding corrections to the measured values introduced some uncertainties that may vary from isotope to isotope, but above  $\sim 400$  keV the corrections are small in all cases and the associated uncertainties are considerably smaller than the above systematic  $^{182}\text{W}$  discrepancy. The "base" model gives a good description of the measured angle-integrated elastic-scattering cross sections of all three isotopes over the entire measured energy range as illustrated in Fig. IV-1. For all three isotopes the calculated angle-integrated cross sections for the excitation of the first  $2+$  states are somewhat larger than experimentally observed at low energies (e.g. by 5-10% below  $\leq 1.0$  MeV). At high energies (e.g.  $\geq 3.5$  MeV), where the excitations of the  $2+$  states are essentially entirely due to direct processes, the agreement between calculated and measured values is good. In the intermediate-energy range there are systematic differences that decrease with increasing target mass. Measured and calculated angle-integrated cross sections for the excitations of the first  $4+$  states are in reasonably good agreement for all three isotopes over the energy range where the cross sections are of appreciable magnitude. There is no anomalous behavior of the  $4+$  excitations as, for example, reported in the samarium isotopes (IV-11).

The measured neutron differential-elastic-scattering cross sections are generally compared with those calculated from the "base" model in Fig. IV-2, with some more detailed illustrations given in Figs. IV-5, -6, and -7. On the whole, the agreement is reasonably good. There are some isolated discrepancies, notably in the extreme minima of the distributions. The latter are probably of experimental origin, possibly associated with small experimental-angle uncertainties and/or inappropriate multiple-event corrections in regions where those corrections are very large (IV-12). If there is a systematic discrepancy, it is in the description of  $^{182}\text{W}$  elastic scattering in the mid-angle-energy range where the calculated results are systematically larger than the measured values.

General comparisons of measured and calculated neutron differential cross sections for the excitation of the first  $2+$  and  $4+$  states are shown in Figs. IV-3 and 4 with some more detailed illustrations in Figs. IV-5, 6 and 7. The calculated and measured relative shapes are generally very similar. There is a tendency for the calculated magnitudes, particularly of the  $2+$  excitations, to be smaller than the measured values at lower energies where the compound-nucleus contribution to the cross section is relatively large as noted above. The differential cross sections for the excitation of the  $4+$  states are relatively very small (a few milli-barns per steradian) and, as a consequence, the experimental uncertainties are large making detailed model comparisons less rewarding, particularly at higher energies.

These three isotopes of tungsten are spectroscopically quite different. Each is statically deformed with a characteristic ground-state-rotational band. This is followed by beta- and gamma-vibrational bands. In  $^{182}\text{W}$  the beta-vibrational band head is somewhat above 1.0 MeV followed, at higher energies, by the gamma-vibrational-band. As the target mass increases the gamma-vibrational-band energy decreases, crosses the beta-band, to a relatively low energy of  $\sim 0.75$  MeV in  $^{186}\text{W}$ . These characteristics are evident in Ref. IV-5, outlined in Fig. III-9 and discussed in some detail in Ref. IV-8. Even within this general band framework there are uncertainties, e.g. the results of recent  $(n;n')$ , gamma) measurements are not entirely consistent with the level

structure of  $^{186}\text{W}$  as reported in the compilation of Ref. IV-5 (IV-8). These large changes in collective structures have possible implications on the direct interactions associated with the present interpretations as discussed below. Even in the simpler context of compound-nucleus reactions the situation is complicated by the realities of experimental resolutions which preclude the explicit determination of the cross sections associated with isolated levels at excitations much above 1.0 MeV and by uncertainties associated with the underlying structure itself.

The calculation of cross sections for excitations above the ground-state rotational band generally assumed the correlation between observed and underlying structure outlined in Table IV-2 and that the cross sections were due entirely to the compound-nucleus process. Possible direct-reaction contributions are discussed below. The calculated results are compared with the measured values in Figs. IV-8, 9 and 10. Generally, the agreement between measurement and calculation is better for the lower-energy excitations and the heavier target masses. There is a trend, also evident in the excitation of the ground-state rotational bands shown in Fig. IV-1, for the calculated results to be smaller than the measured values in the mid-energy regions and increasingly so for decreasing target mass. The differences are most evident in  $^{182}\text{W}$  where more reliance had to be placed upon statistical level distributions in the calculation of compound-nucleus channel competition. These considerations suggest that for these particular targets and this energy range the level density model of Gilbert and Cameron results in excessive channel competition. Similar problems have been encountered in other mass regions at approximately the same excitation energies (IV-13). The situation can be considerably improved by adjusting the level density parameters in such a way as to reduce channel competition but such adjustment is largely pragmatic and thus was not pursued here. It was concluded that the simple statistical representation of Ref. IV-6 was an over-simplification in the present context which generally resulted in the calculation of significantly too small compound-nucleus cross sections over much of the mid-energy range of the present measurements.

Beyond the general impressions, above, there are some specific characteristics evident in Figs. IV-8, 9 and 10. The calculated excitations of the first 6+ states are all smaller than the measured values; e.g. those for the 671 keV level of  $^{182}\text{W}$ . However, the cross sections are very small (few milli-barns per steradian) and it is likely that they were over estimated in the measurements. The calculated values for the weakly excited  $^{182}\text{W}$  beta-band head at 1138 keV are reasonably consistent with the measured values. The observed strong excitation of levels at 1.2-1.3 MeV in  $^{182}\text{W}$  is due to several 2+ levels and the calculations are reasonably consistent with the limited experimental results. It is difficult to correlate measured and calculated excitations in  $^{182}\text{W}$  above  $\sim 1.3$  MeV and it seems likely that there were a number of additional components contributing to the measured values not included in the calculational model. The comparisons of measured and calculated excitations in  $^{184}\text{W}$  and  $^{186}\text{W}$  are somewhat analogous and in both the agreement tends to be better than for  $^{182}\text{W}$ . This is particularly so for  $^{186}\text{W}$  where the levels are reasonably known and where the experimental definition is good to  $\sim 1.0$  MeV.

One conspicuous calculational shortcoming arises for the  $1182 \pm 26$  keV excitation in  $^{186}\text{W}$ . It will serve to illustrate computational difficulties encountered in the quantitative representation of higher excitations in these isotopes. The state in question has been observed at this laboratory in a number of measurements over a period of years and gross errors in excitation energy as well as cross section magnitude seem unlikely. Although somewhat outside the excitation energy error, the known level at  $E_x = 1150$  keV,  $J^\pi = 0^+$  (Ref. IV-5) appears to be the most plausible identification. However, the cross sections calculated using this spin are roughly a factor of two below the experimental values (see Fig. IV-10). Consideration of the  $4^-$  member of the octupole-vibrational band, expected to lie near this energy, does not improve the calculated result. These observations suggested the inclusion of a  $2^+$  level at approximately 1180 keV and this approach met with success (see Ref. IV-8). Indeed, recent interacting-boson model calculations (Ref. IV-16) suggest a  $2^+$  level at 1156 keV with small  $B(E2)$  coefficients for transitions from this state to both the  $E_x = 122$  keV,  $J^\pi = 2^+$  level and the ground state. On the other hand, preliminary study of gamma-rays emitted following fast-neutron bombardment of  $^{186}\text{W}$  by one of the authors (P.T.G.) indicates a strong transition from a surmised  $1153 \pm 2$  keV level to the 122 keV ( $2^+$ ) level, while no companion ground state transition was found. This observation favors the  $J^\pi = 0^+$  assignment. Further, no suitable transitions could be identified to justify the assumption of the postulated  $2^+$  level near 1180 keV. Hence there appears to be no satisfactory explanation at this time for this apparent discrepancy between calculation and experiment.

It is not attractive to attempt to extend the comparisons of measured and calculated cross sections to levels above  $\sim 1.5$  MeV excitation energy. The observed inelastically-scattered neutron groups very likely consist of contributions from a number of poorly defined levels, the properties of which are essentially unknown. It is also doubtful that spectroscopic information can be reasonably construed from the present experimental results for levels much above  $\sim 1.0$  MeV excitation energy because of the same shortcomings in experimental definition and knowledge of underlying level structure.

As noted above, the "base" model does not properly describe the observed neutron total cross sections of  $^{182}\text{W}$  at lower energies. This is disturbing as these cross sections are among the more reliable of calculated and measured quantities. Assuming the general validity of the model, one seeks parameters unique to  $^{182}\text{W}$  for the origin of the discrepancy. Prominent of these are the quadrupole and hexadecapole deformations. Elastic-scattering distributions are very sensitive to the choice of beta-4, as discussed in Ref. IV-8, and appreciable variations in this parameter are not attractive. An alternative is the quadrupole deformation, which if reduced from the value of 0.223 given in Ref. IV-7 to  $\sim 0.205$  (a value essentially the same as that of the other two isotopes) considerably improves the calculated description of the low-energy total cross sections of  $^{182}\text{W}$  as illustrated in Fig. IV-11. Concurrently there is a marginal improvement in the description of the cross sections for the excitation of the first  $2^+$  state in  $^{182}\text{W}$ . The description of large angle elastic scattering is also improved but at some compromise of the agreement with the measured values in the mid-angle range as illustrated in Fig. IV-12. These observations, based essentially upon comparisons of measured and calculated total cross sections, could suggest that the quadrupole deformation

of  $^{182}\text{W}$  is less than given in Ref. IV-7 and the recent compilation of Ref. IV-14. This suggestion is speculative and not consistent with other experimental evidence or the notion that the tungsten isotopes lie in a region of transition from deformation to sphericity. Perhaps it reflects some other aspects of collective deformation such as alternate coupling schemes or higher-order deformations not addressed in the above calculations.

The above calculations employed the width-fluctuation and correlation enhancement correction factors defined by Moldauer (IV-4). These correction factors use a channel degree of freedom of  $\nu \approx 1.8$  resulting in an elastic enhancement factor of  $\sim 2.1$ . The values are very sensitive to the statistical assumptions both as regards resonance pole-residue amplitudes and pole spacings. Alternate choices of  $\nu$  are possible and the choice can significantly effect the cross section calculations involving appreciable compound-nucleus components. This sensitivity was examined by assuming  $\nu = 1.0$  and repeating the above calculations in regions where the compound-nucleus contribution is large. The results are indicated by the "C" curves in Fig. IV-1. In the low-energy, few-channel region the enhancement of the elastic scattering cross section increases but the values remain consistent with the experimental results to within the measurement uncertainties. Concurrently, the calculated cross sections for the prominent excitations of the first  $2^+$  states are reduced by 5-10% bringing them into better agreement with the measured values. Other illustrations of the effect of the choice of  $\nu$  are given in Ref. IV-8. The choice of parameters underlying the correction factors is not, a priority, readily determined and yet it can significantly effect the calculated result. Thus, the capability to quantitatively calculate compound-nucleus cross sections remains appreciably predicated on the pragmatic adjustment of correction parameters to achieve agreement with experimental values.

The possibility of direct-reaction contributions to the inelastic excitations beyond the ground state rotational band (GSRB) was explored. Before entertaining these considerations it should be immediately pointed out that the proper investigation of coupling schemes beyond the GSRB requires a detailed redetermination of all optical model parameters. This massive effort was judged not to be justified at this time for a number of reasons. For example, it will be shown below, that the perturbations to the GSRB caused by these higher-order couplings, while not negligible, are nevertheless small. Further, an exacting definition of the new parameters associated with the various relevant coupling schemes often requires a precision and scope of experimental data beyond that realized in this work. (Examples of useful additional information are the resolution of close-lying members of different rotational bands and the definition of inelastic-neutron angular distributions outside the present angular range, i.e. at very small and very large angles.) In view of these limitations it would appear reasonable to use the base-model parameterization to qualitatively estimate the extent of vibrational-rotational-coupling in inelastic-neutron excitation. The results so derived must be considered qualitative or even speculative.

In terms of cross section magnitude and angular distribution definition the most favorable subject for discussion in the present data set is the gamma-vibrational band (GVB) head in  $^{186}\text{W}$  ( $E_x = 738$  keV and  $J^\pi = 2^+$ ). Its excitation function is identified in Fig. IV-10 by the observed  $E_x = 742$  keV. As the

Figure shows, the calculated compound nuclear (CN) cross section is consistently smaller than that observed experimentally above  $E_n = 1.5$  MeV. While a compound-nucleus correction factor can be invoked to partially explain this shortcoming, (see above remarks), the addition of a direct reaction (DR) component, can also be considered. Support for this contention may be found in the angular distributions of neutrons scattered from this state. In Fig. IV-13 the distributions at  $E_n = 2.5$  MeV are depicted for three neighboring inelastic excitations, identified by average experimental excitation energies. They are the GVB head at 742 keV, the octupole-vibrational band head at 950 keV and the composite group at 858 keV consisting of the second GVB member ( $E_x = 862$  keV,  $J^\pi = 3^+$ ) and the beta-vibrational band (BVB) head ( $E_x = 882$  keV,  $J^\pi = 0^+$ ). These distributions as well as those shown in Fig. IV-15) are composites of many distributions obtained over several years. In order to retain as much shape information as possible, they were arbitrarily normalized before combining and interpolating to a standard angle set. The resultant averaged distributions were then renormalized to the smoothed, energy-averaged integral cross section implied by the data of Fig. IV-10. The curves labelled "C" in Fig. IV-13 are the CN shapes derived from spherical statistical-model calculations discussed in the beginning of this section. They have been scaled to best fit the data and thus indicate their ability to represent the angular distributions. They do reasonably well for the 858 and 950 keV excitations but are obviously not sufficiently anisotropic in the case of the GVB head. The curves labelled "C + D" contain DR components, as explained below, and conform better with the shapes suggested by the data.

In calculating the angular distributions for the various vibrational band excitations it was assumed, as before, that the DR and CN components were separately calculable. The CN shapes were taken from the spherical calculations described above. The DR components were computed with JUSTSO (Ref. IV-2) employing two coupling schemes:

Case A: GSRB ( $0^+, 2^+, 4^+$ ) + GVB ( $2^+, 3^+$ )

Case B: GSRB ( $0^+, 2^+, 4^+$ ) + GVB ( $2^+, 3^+$ ) + BVB ( $0^+$ ).

The actual states coupled are indicated parenthetically by their respective spins. The coupling-strength parameters,  $\eta$ , (see Ref. IV-15) required for each vibrational band were treated as empirical parameters. An example of the coupled-channels calculations is shown in Fig. IV-14. Case A employed  $\eta_{GVB} = 0.1$ , while case B employed  $\eta_{GVB} = 0.2$  and  $\eta_{BVB} = 0.1$ . Part (b) shows the resultant DR components for the vibrational bands. The shapes for the GVB  $2^+$  state are rather similar and, when diluted with the CN shape, they clearly strain the analyzing power of the available data. Part (a) indicates the attendant perturbations to the GSRB. These correspond to relatively small variations in optical model parameters (see Ref. IV-8). For example, a 25% change in  $\beta_4$  could correct much of the deviations exhibited by DR components of the  $0^+$  and  $2^+$  angular distributions. The corresponding change in the total cross section is  $\sim 1\%$ . Furthermore, changes such as that of the  $2^+$  member of the GSRB are easily marked by uncertainties in the width-fluctuation correction as noted above. However, in the end, the feasibility of these parameter adjustments must be judged with all relevant data in mind.

The superposition of the DR and CN components was effected by simultaneously adjusting their amplitude to the data in the least-squares sense. This seemingly ad-hoc procedure can be justified with respect to the DR component by noting that small variations in the coupling strength  $\eta$  primarily affect the angular distribution magnitude rather than its shape. The procedure was carried out for the GVB head at several energies between  $E_n = 1.8$  and 3.0 MeV and gave multipliers for the CN and DR components that were consistent to  $\sim \pm 10\%$  with the exception that at 1.8 MeV where the CN multiplier was considerably larger than unity (i.e. 1.3) for both cases. In addition the multiplier for the DR component of case A showed a decrease with energy as already observed in Ref. IV-8. This initial assay implied coupling strengths for case A ranging roughly from  $\approx 0.13$  to 0.06, while for case B a constant  $\eta_{\text{GVB}} \approx 0.15$  was adequate. These values should be taken with considerable reservation in view of the crudeness of their derivation. Nevertheless, coupled-channels calculations were repeated for these coupling strengths. The resultant DR components, the CN components and their sum are shown for three energies in Fig. IV-15. At  $E_n = 1.8$  MeV the data favor the symmetry of case A. However, at  $E_n = 2.5$  MeV case B has become the better choice. At  $E_n = 3.0$  MeV case A gives a very poor fit (it has not been shown), whereas case B proves to be quite satisfactory. Even so, the forward peaking of the data is not entirely reproduced, the rather larger error of the first data point notwithstanding. The fact that case B gives an energy-independent coupling strength also weighs strongly in its favor. One further bit of support for case B results from the addition of DR components for the  $0^+$  and  $3^+$  states convoluted in the 858 keV group. Doing so produces a slight bump near  $\sim 90^\circ$  which the data seem to exhibit in Fig. IV-13 and which the CN component alone does not possess.

The conclusion to be drawn from the foregoing discussion is that the more complex (but hopefully physically more realistic) coupling scheme, case B, is evidently more successful in reproducing the overall trends indicated by the data. Not only do these calculations conform to the shapes of the angular distributions but they also give a reasonably coherent account of cross section magnitudes. It is interesting to note that the amplitude of the DR component declines with increasing energy. It has been repeatedly stressed that the consequences of this revised coupling scheme must be considered in the context of the entire data base in order to be rigorous. Conversely (and this may well be the most important conclusion of this portion of the study), the physical significance of model-parameterization refinements are dependent upon the delineation of physically realistic coupling schemes.

Table IV-1. Base Tungsten Potential Parameters taken from Ref. IV-7.

---

Real Potential

$$V = 49.90 - 16 \left( \frac{N-Z}{A} \right) - 0.25 E \quad \text{MeV}$$

$$R = 1.26 \quad \text{F}$$

$$A = 0.63 \quad \text{F}$$

Imaginary Potential

$$W = 4.93 - 8 \left( \frac{N-Z}{A} \right) + 1.3 E^{1/2} \quad \text{MeV}$$

$$R = 1.28 \quad \text{F}$$

$$A = 0.47 \quad \text{F}$$


---

Where

All radii are equal to  $R \cdot A^{1/3}$ .

The real potential has the Saxon form.

The Imaginary potential is the surface-derivative of the Saxon form.

The spin-orbit strength is taken to be 6.0 MeV.

Quadrupole deformations are 0.223 (182), 0.209 (184) and 0.203 (186).

Hexadecapole deformations are -0.054 (182), -0.056 (184) and -0.057 (186).

Table IV-2. Level Structure used in Comparing Observed Neutron Inelastic Excitations with Calculations.

$E_x^a(J-\pi)$	$E_x^a(J-\pi)$	$E_x^a(J-\pi)$
$^{182}\text{W}$	$^{184}\text{W}$	$^{186}\text{W}$
671 (6+)	737 (6+)	742 (2+)
1138 (0+)	905 (2+)	858 (6+, 3+, 0+)
1229 + 1281 (2+, 2-, 2+)	1000 (0+, 3+)	950 (2-)
1309 + 1357 (3+, 3-)	1125 (2+, 2-, 4+)	1028 (2+, 4+, 4-, 3-)
1428 (4+)	1237 (3-, 5-, 5+, 0+)	1182 (0+)
1492+ (4-, 4+, 4-)		1296 (1-, 2+, 2+, 2+)

<sup>a</sup>Excitation energies in keV,  $J^\pi$  assignments taken from Ref. IV-5.

References, Section IV.

- IV-1. T. Tamura, Rev. Mod. Phys., 37, 679(1965).
- IV-2. JUSTSO, a coupled-channels computational program, P. Moldauer, Private Communication, (1980).
- IV-3. W. Hauser and H. Feshbach,, Phys. Rev., 87, 366(1952).
- IV-4. P. A. Moldauer, Nucl. Phys., A344 185(1980); see also Phys. Rev., C12 744(1975).
- IV-5. Table of Isotopes, 7th Ed., Eds. C. Lederer and V. Shirley, John Wiley and Sons, New York (1978).
- IV-6. A. Gilbert and A. Cameron, Can. Jour. Phys., 43, 1446(1965).
- IV-7. J. P. Delaroche, G. Haouat, J. Lachkar, Y. Patin, J. Sigaud and J. Chardine, Proc. Conf. Nucl. Cross Sections for Technology, Natl. Bureau of Stds. Pub., NBS-SP-594 (1980).
- IV-8. P. T. Guenther, "The elastic and inelastic scattering of fast neutrons from the even isotopes of tungsten," Thesis, University of Illinois (1977).
- IV-9. D. Lister, A. Smith and C. Dunford, Phys. Rev., 162 1077(1967).
- IV-10. P. Moldauer, Neutron Strength Functions, The Link between Resolved Resonances and the Optical Model, Conf. on Methods of Evaluation, Brookhaven National Laboratory, (1980).
- IV-11. P. Guenther, W. Poenitz and A. Smith, Conf. on Methods of Evaluation, Brookhaven National Laboratory (1980).
- IV-12. D. Coope, S. Tripathi, M. Schell, J. Weil and M. McEllistrem, Phys. Rev., C16 2223(1977).
- IV-13. A. Smith, Private Communication (1980).
- IV-14. P. Möller, Nucl. Phys., A192 529(1972).
- IV-15. T. Tamura, ORNL Report No. 4152 (1967), Appendix A.
- IV-16. B. Barrett, Private Communication (1981).

Figure Captions, Section IV.

- Fig. IV-1. Comparison of measured and calculated neutron cross sections of  $^{182}\text{W}$ ,  $^{184}\text{W}$  and  $^{186}\text{W}$ . The measured values are indicated by data symbols as follows:  $+$  = total cross sections,  $0$  = elastic scattering,  $\square$  = inelastic excitation of the first  $2+$  state and  $X$  = inelastic excitation of the first  $4+$  state. The light "B" curve is an eye-guide constructed through the experimental results of Ref. IV-9 as described in the text. Heavy curves denote the results of calculations; "A" (or unmarked) are results obtained with the "base" model described in the text and "C" are results obtained with modified compound-nucleus corrections as defined in the text.
- Fig. IV-2. Comparison of measured and calculated neutron differential-elastic-scattering cross sections of  $^{182}\text{W}$ ,  $^{184}\text{W}$  and  $^{186}\text{W}$ . Experimental results are indicated by data points and the results of calculations using the "base" model of the text by curves.
- Fig. IV-3. Comparison of measured and calculated neutron-differential-scattering cross sections for the excitation of the first  $2+$  states of  $^{182}\text{W}$ ,  $^{184}\text{W}$  and  $^{186}\text{W}$ . The experimental results are indicated by data symbols and those obtained via calculation by curves.
- Fig. IV-4. Comparison of measured and calculated neutron-differential-scattering cross sections for the excitation of the first  $4+$  states of  $^{182}\text{W}$ ,  $^{184}\text{W}$  and  $^{186}\text{W}$ . The experimental results are indicated by data symbols and those obtained via calculation by curves.
- Fig. IV-5. Illustrative comparisons of measured and calculated differential-scattering cross sections of  $^{182}\text{W}$ . Curves indicate the results of calculation; data points the experimental values defined as follows:  $\square$  = elastic scattering,  $0$  = inelastic excitation of the first  $2+$  level, and  $X$  = inelastic excitation of the first  $4+$  level. The incident neutron energies in MeV are numerical given in each section of the figure. The dimensionality is cross section in b/sr and scattering angle in lab.-deg.
- Fig. IV-6. Illustrative comparisons of measured and calculated differential-scattering cross sections of  $^{184}\text{W}$ . The notation is identical to that of Fig. IV-5.
- Fig. IV-7. Illustrative comparisons of measured and calculated differential-scattering cross sections of  $^{186}\text{W}$ . The notation is identical to that of Fig. IV-5.
- Fig. IV-8. Comparison of measured and calculated neutron inelastic excitation cross sections of  $^{182}\text{W}$ . The data points represent the measured values corresponding to the observed excitation energies noted in keV on the various sections of the figure. The curves indicate the results of calculations as described in the text.

Figure Captions, Section IV. (Contd.)

- Fig. IV-9. Comparison of measured and calculated neutron inelastic excitation cross sections of  $^{184}\text{W}$ . The data points represent measured values corresponding to the observed excitation energies noted in keV on the various sections of the figure. Curves indicate the results of calculations as described in the text.
- Fig. IV-10. Comparison of measured and calculated neutron inelastic excitation cross sections of  $^{186}\text{W}$ . The data points represent measured values corresponding to the observed excitation energies noted in keV on the various sections of the figure. Curves indicate the results of calculations as described in the text.
- Fig. IV-11. Comparison of measured and calculated (with  $\beta_2 = 0.205$ ) neutron cross sections of  $^{182}\text{W}$ . Measured values are indicated by symbols as follows: + = neutron total cross sections, 0 = neutron elastic scattering cross sections,  $\square$  = cross sections for the excitation of the first  $2^+$  state, and X = cross sections for the excitations of the first  $4^+$  state. Curves "A" (and unmarked) denote the calculated results. Curve "C" indicates the calculated result obtained with the alternate formulation of the resonance fluctuation and correlation corrections as described in the text. Curve "B" indicates the low-energy experimental neutron total cross sections results derived from Ref. IV-9.
- Fig. IV-12. Measured and calculated differential-neutron-elastic-scattering cross sections of  $^{182}\text{W}$  at an incident neutron energy of 3.5 MeV. The measured values are indicated by circular symbols. The simple curve is the result of calculations using  $\beta_2 = 0.223$  and the curve with "tick" marks results was obtained with  $\beta_2 = 0.205$ . Dimensionality is b/sr and  $\theta$  in lab.-deg.
- Fig. IV-13. The Angular Distributions of 2.5 MeV Neutrons Inelastically Scattered from  $^{186}\text{W}$ . The distributions are identified by their mean experimental excitation energies. The label "C" refers to compound nuclear angular shapes as given by spherical compound-nucleus calculations. The label "C + D" refers to the superposition of compound nuclear and direct reaction components as described in the text. (Units: b/sr, lab.-deg.).
- Fig. IV-14. The Coupled-Channels-Calculated Direct Reaction Angular Distributions of 2.5 MeV Neutrons Scattered from  $^{186}\text{W}$ . The label "O" refers to the coupling scheme involving only the first three members of the ground state rotational band. The label "A" refers to the coupling scheme of "O" plus the first two members of the gamma-vibrational band. The label "B" refers to the coupling scheme of "A" plus the  $\beta$ -vibrational band head. Part (a) shows angular distributions for the first two members ( $0^+$ ,  $2^+$ ) of the ground state rotational band, while part (b) indicates those for the first two members ( $2^+$ ,  $3^+$ ) of the gamma-vibrational band and the beta-vibrational band head ( $0^+$ ). See text for details. (Units: b/sr, lab.-deg.).

Figure Captions, Section IV. (Contd.)

Fig. IV-15. The Angular Distributions of 1.8, 2.5 and 3.0 MeV Neutrons Scattered from the Gamma-Vibrational Band Head in  $^{186}\text{W}$ . The label "C" refers to the angular-distribution shape given by spherical compound-nucleus calculations. The labels "A" and "B" refer to the direct-reaction angular distribution shapes calculated by the coupled-channels method using coupling schemes A and B as defined in Fig. IV-14. The labels "C + A" and "C + B" identify the sums of compound nuclear and direct-reaction components as described in the text. (Units: b/sr, lab.-deg.).

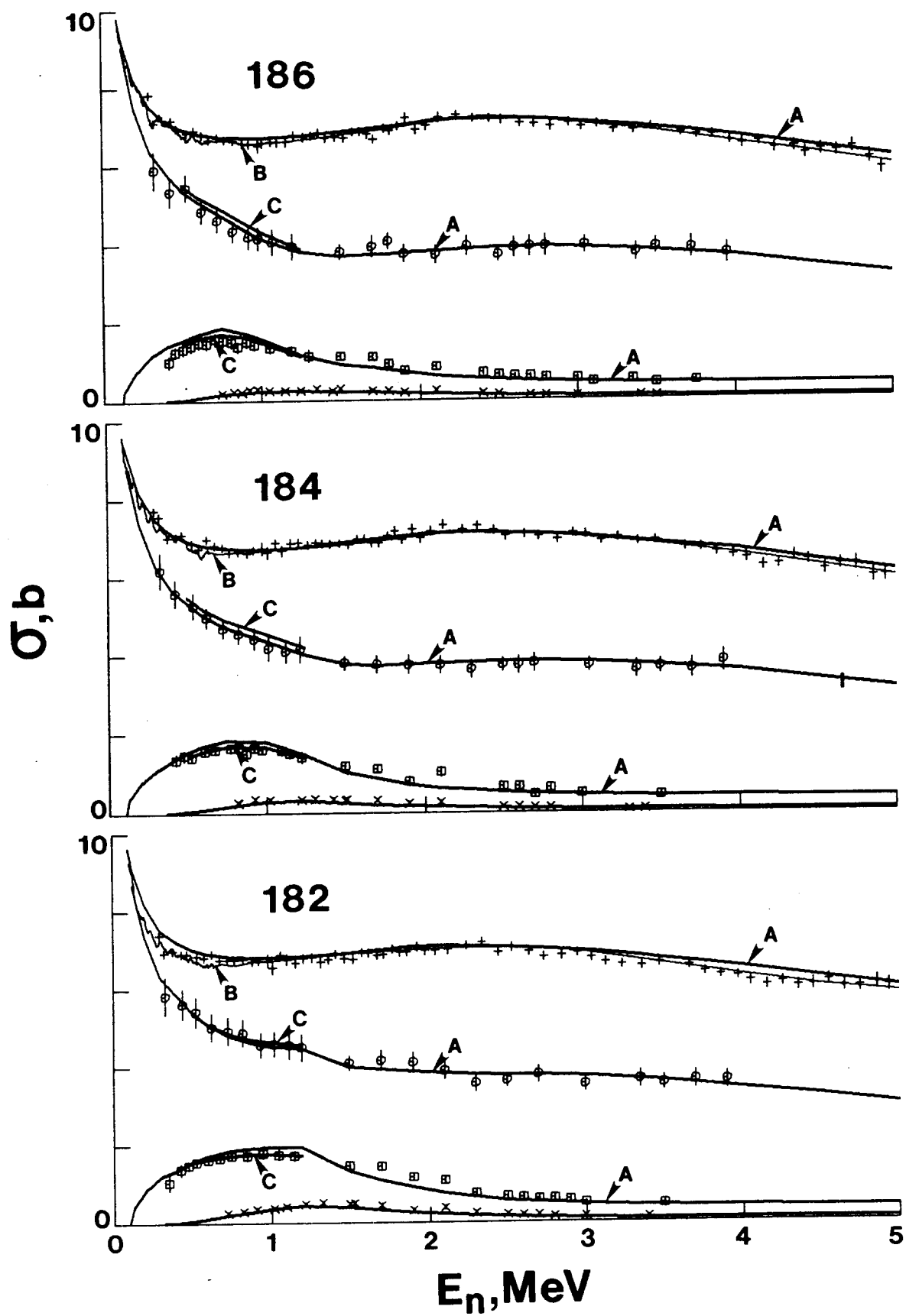


Fig. IV-1.

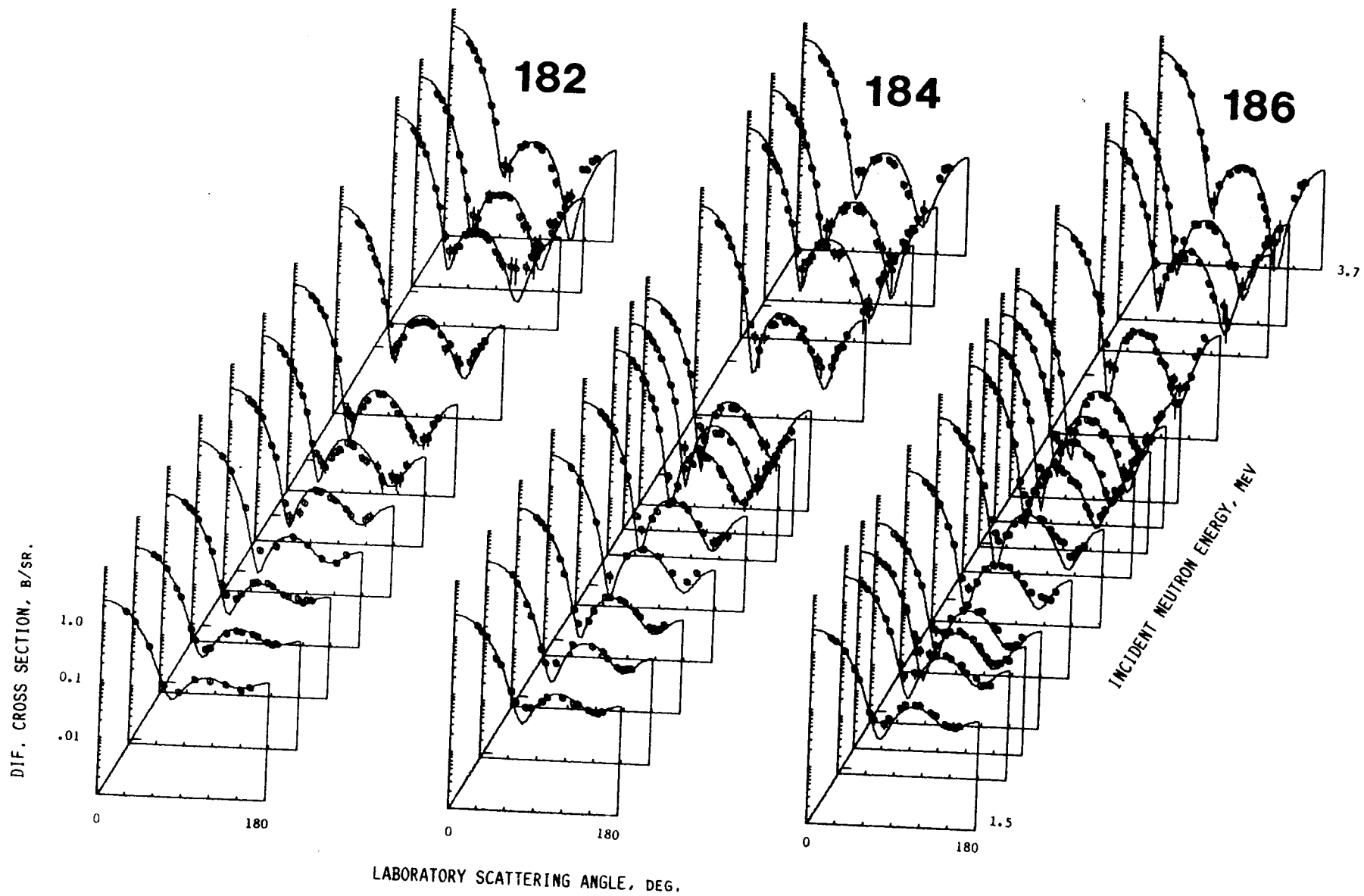


Fig. IV-2.

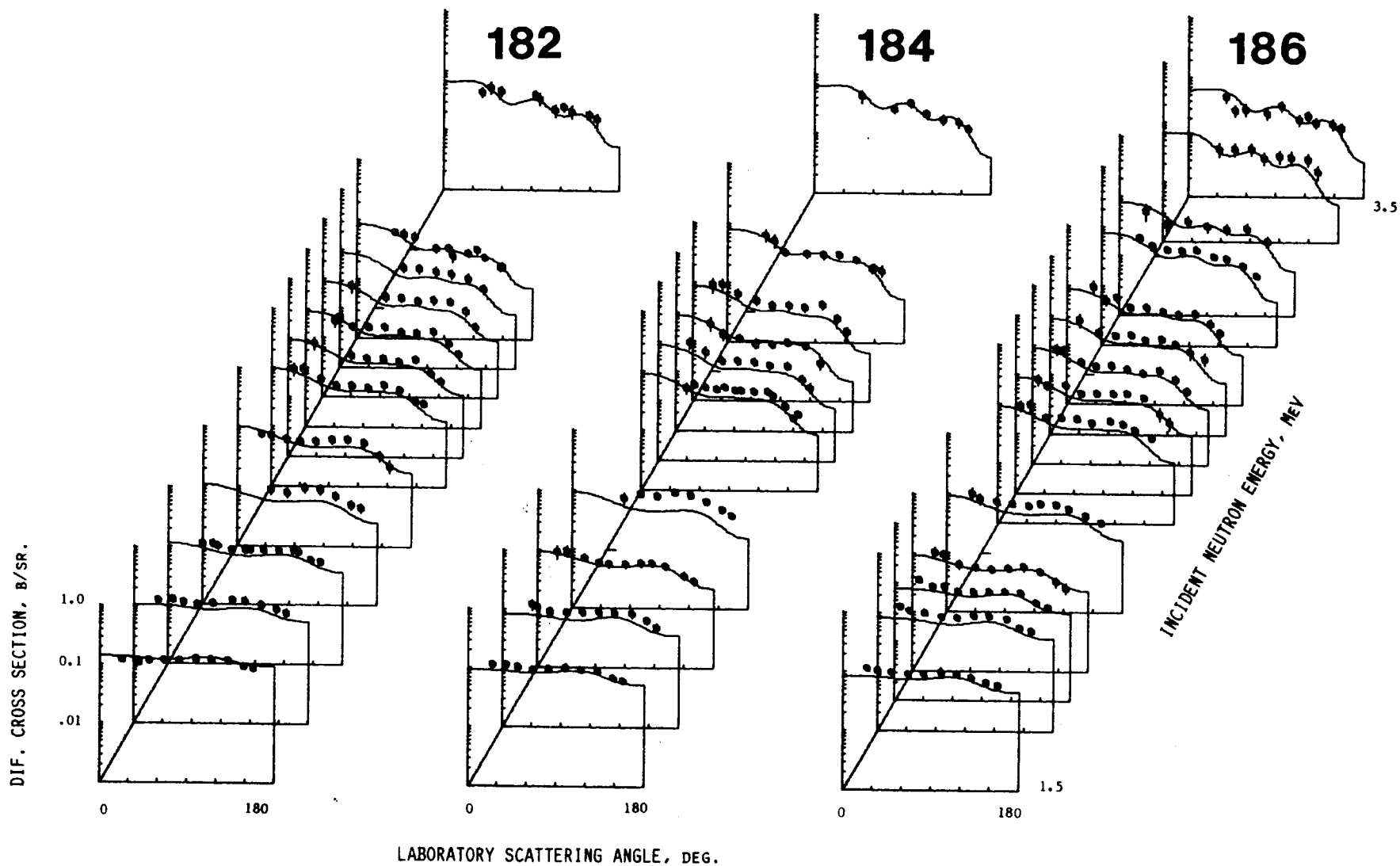


Fig. IV-3.

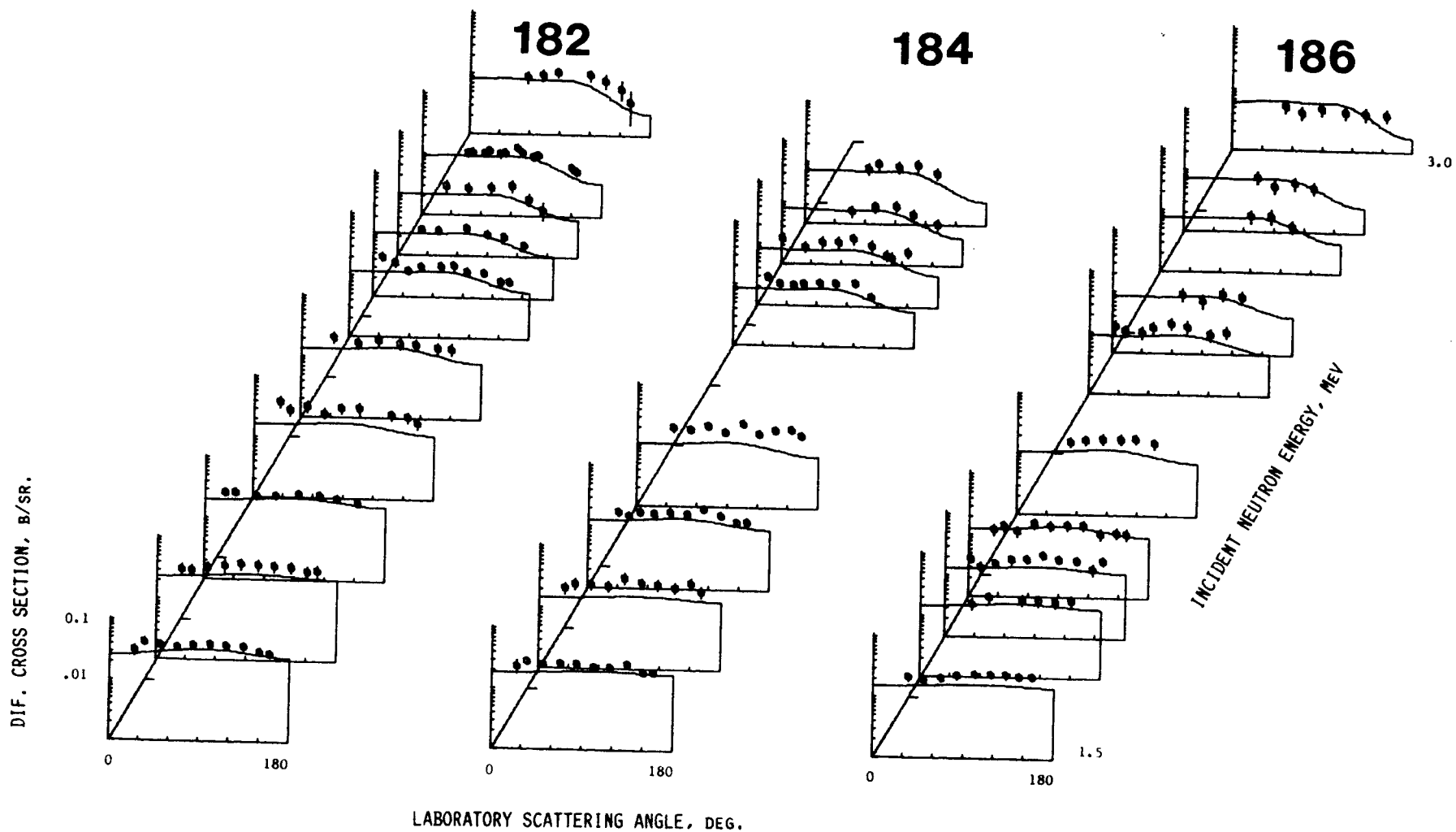


Fig. IV-4.

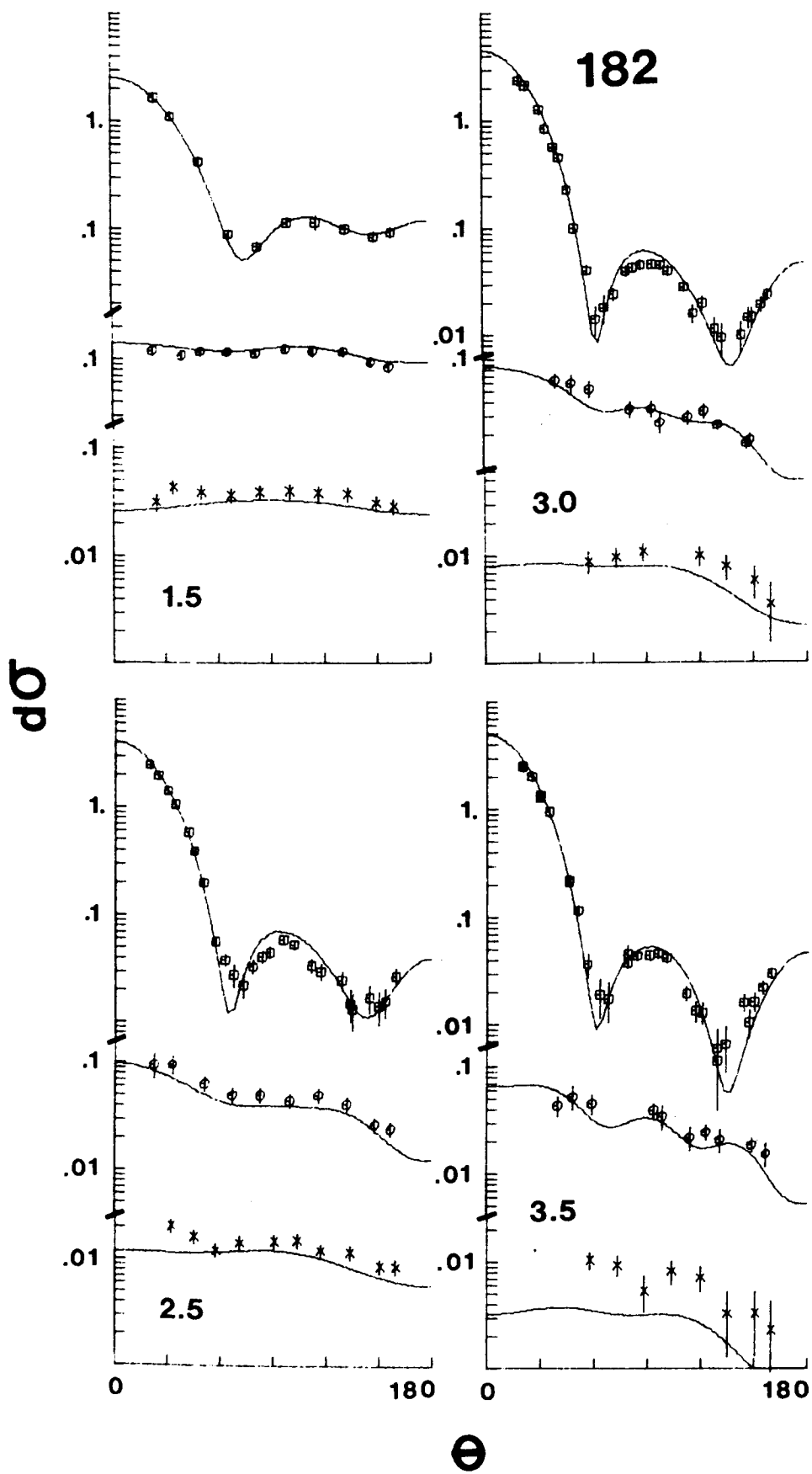


Fig. IV-5.

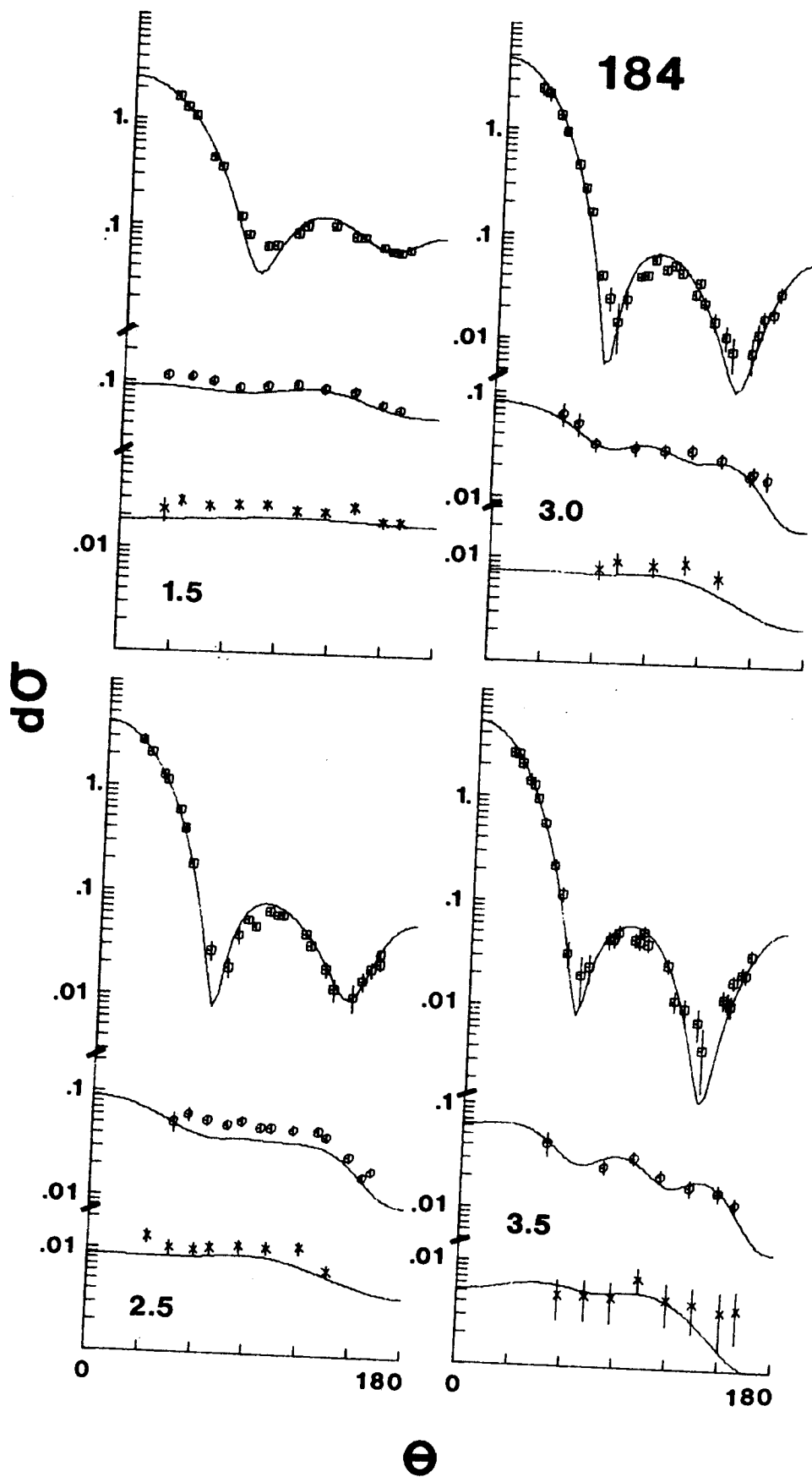


Fig. IV-6.

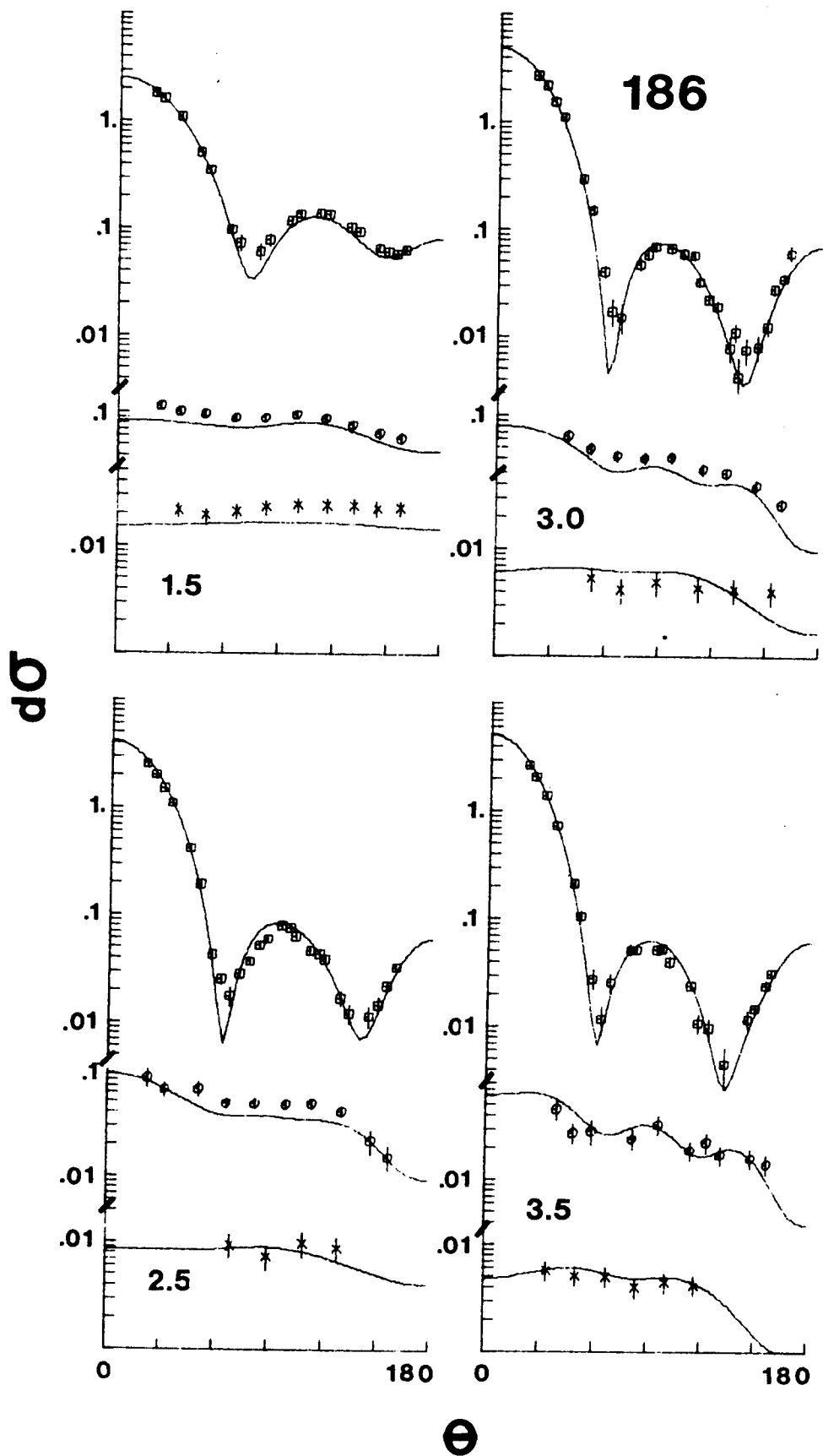


Fig. IV-7.

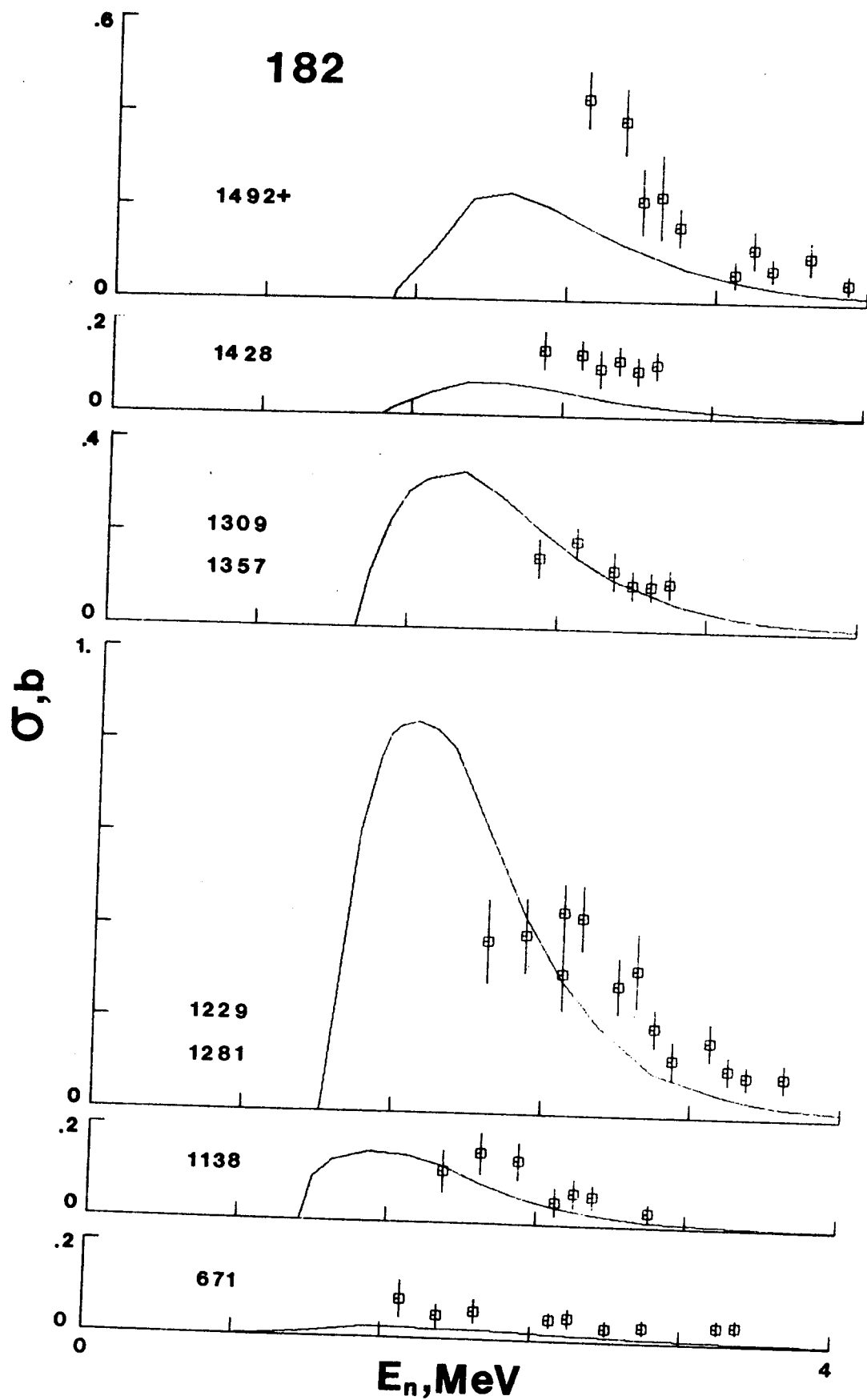


Fig. IV-8.

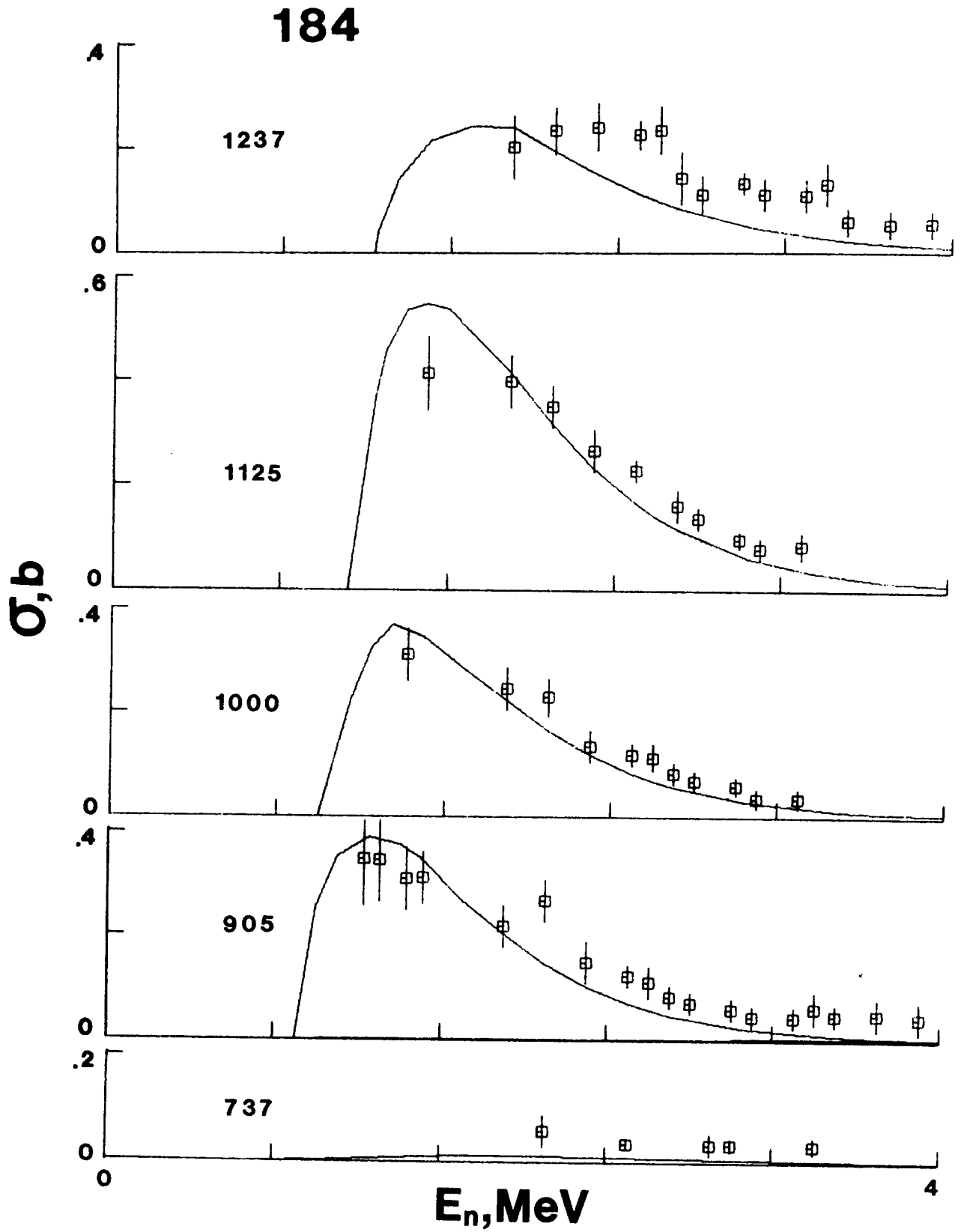


Fig. IV-9.

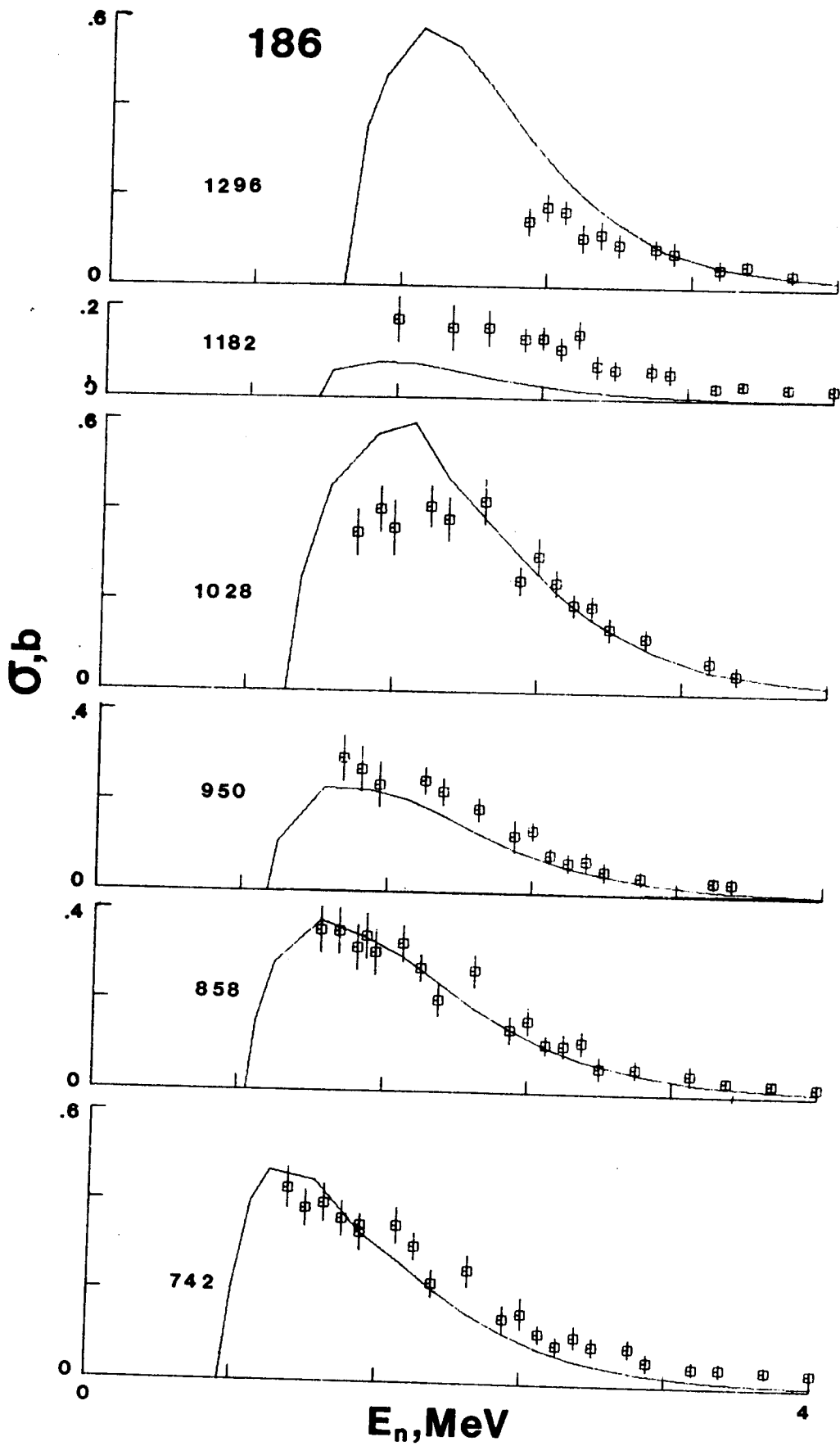


Fig. IV-10.

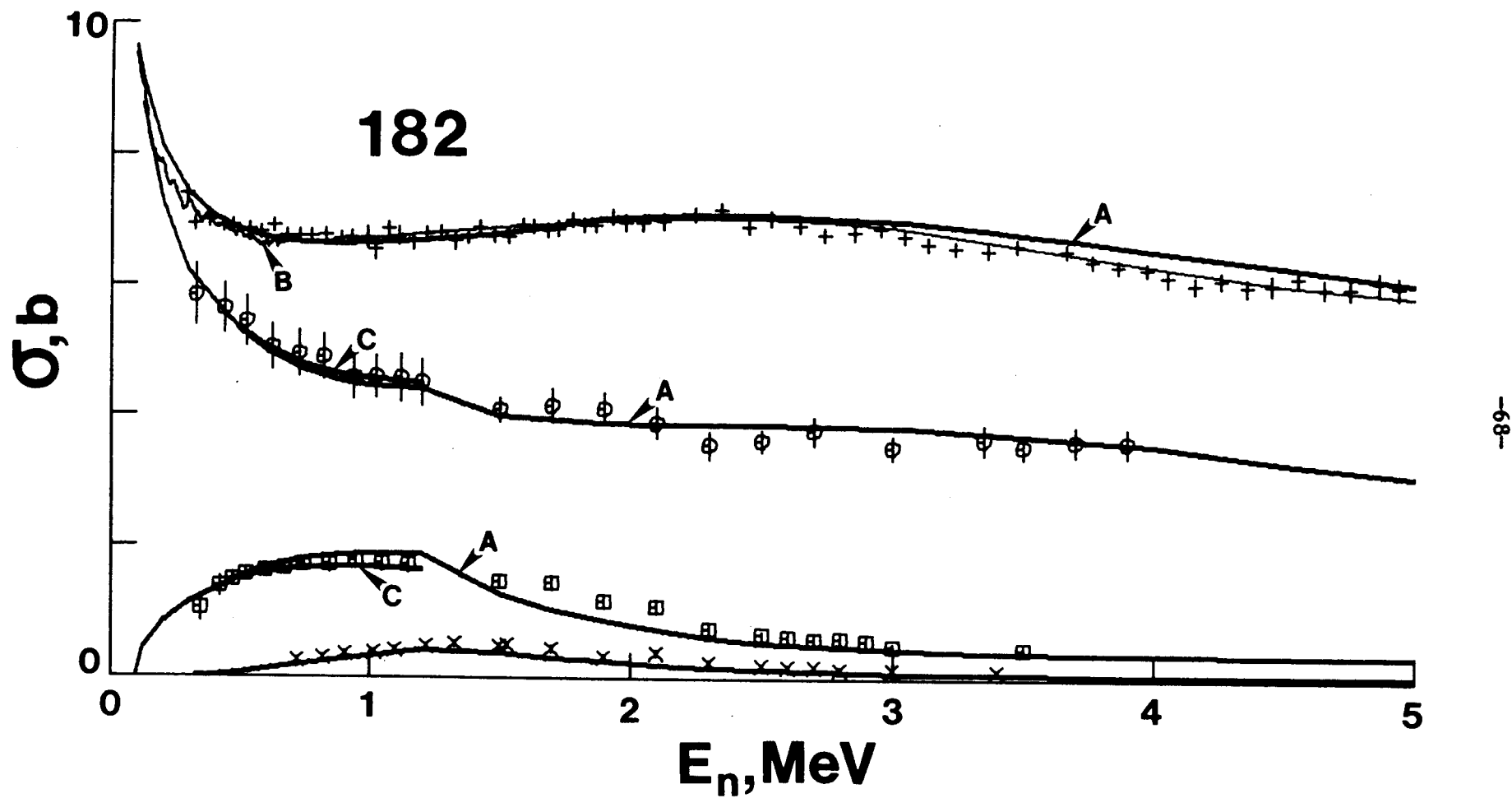


Fig. IV-11.

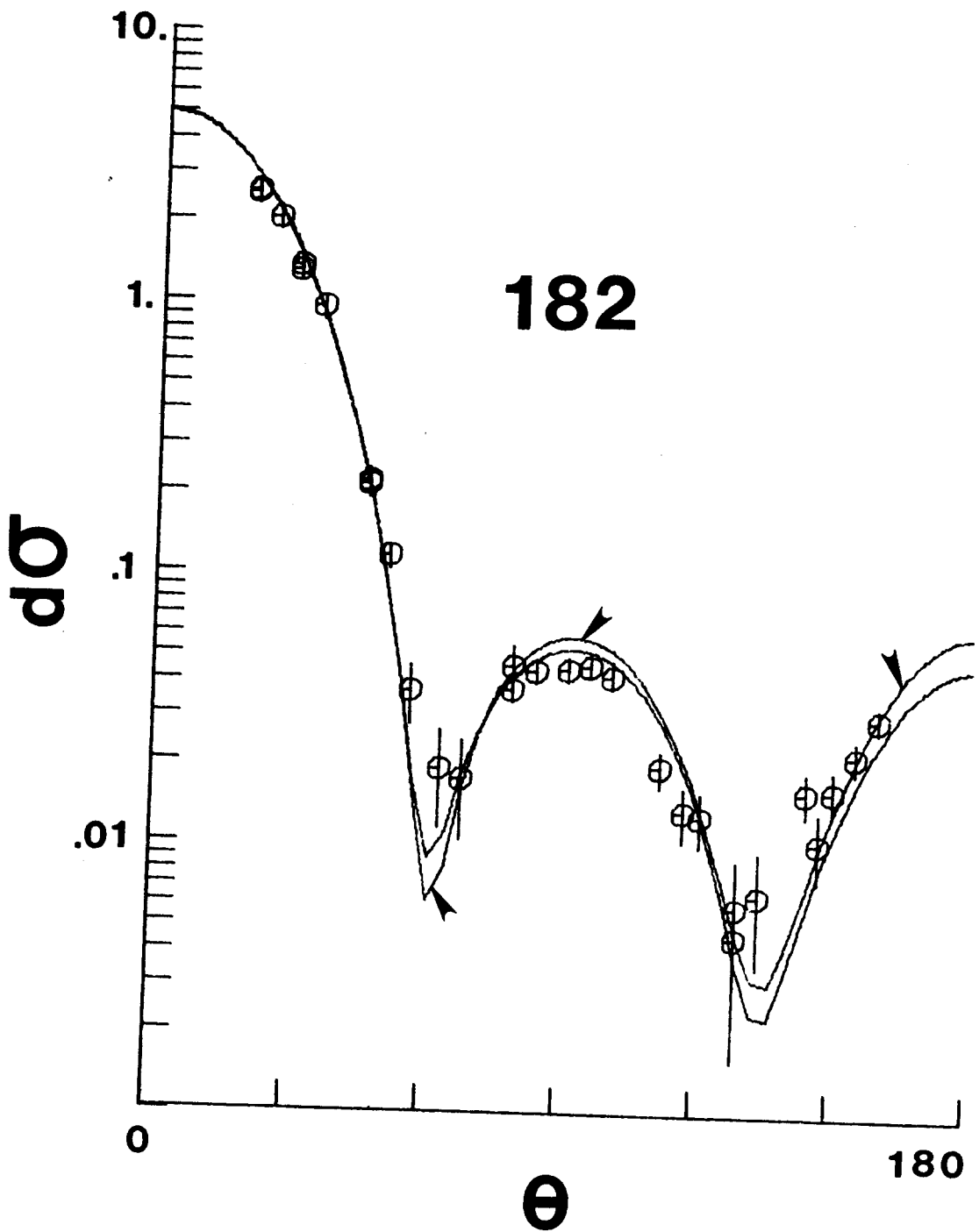


Fig. IV-12.

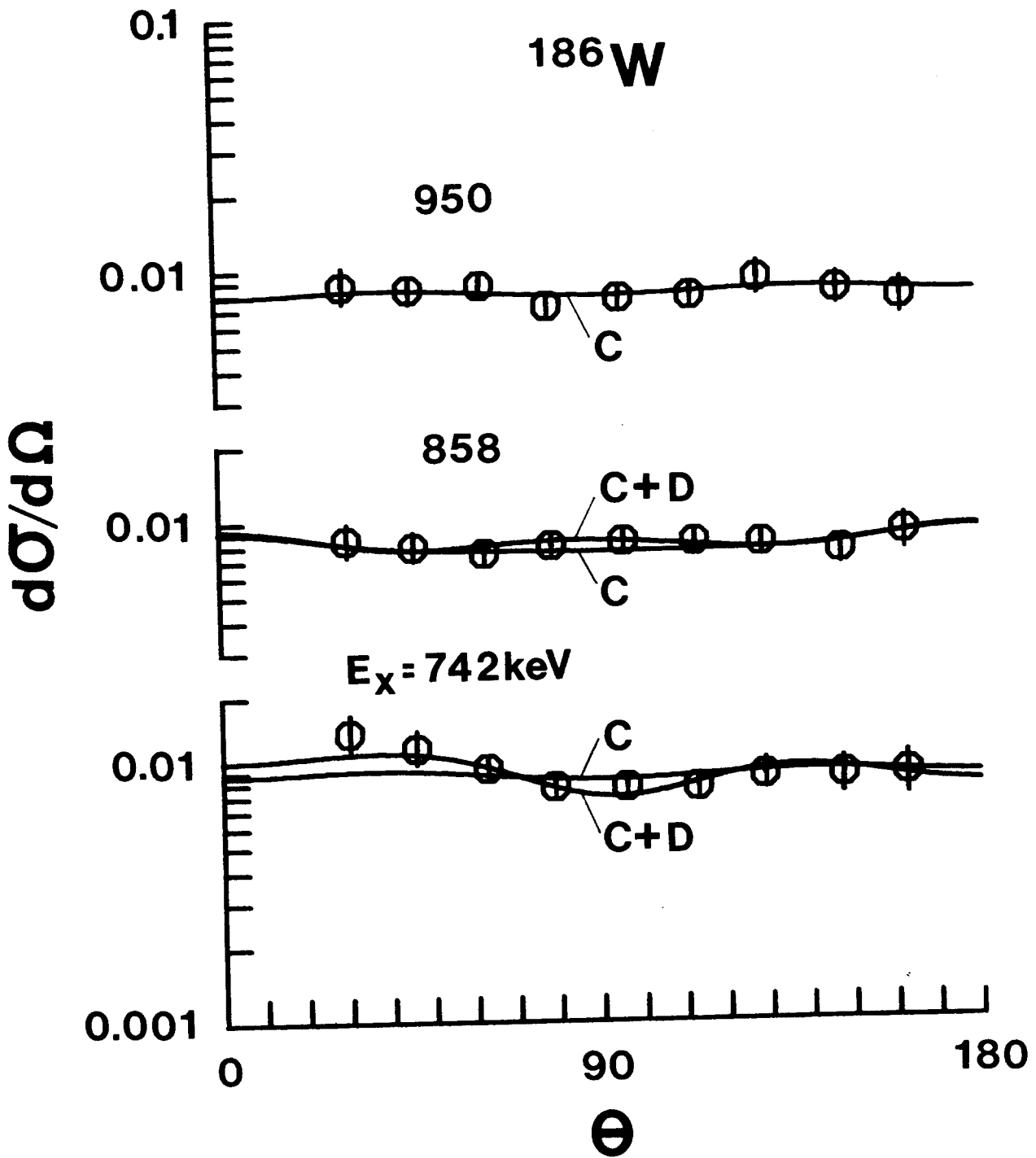


Fig. IV-13.

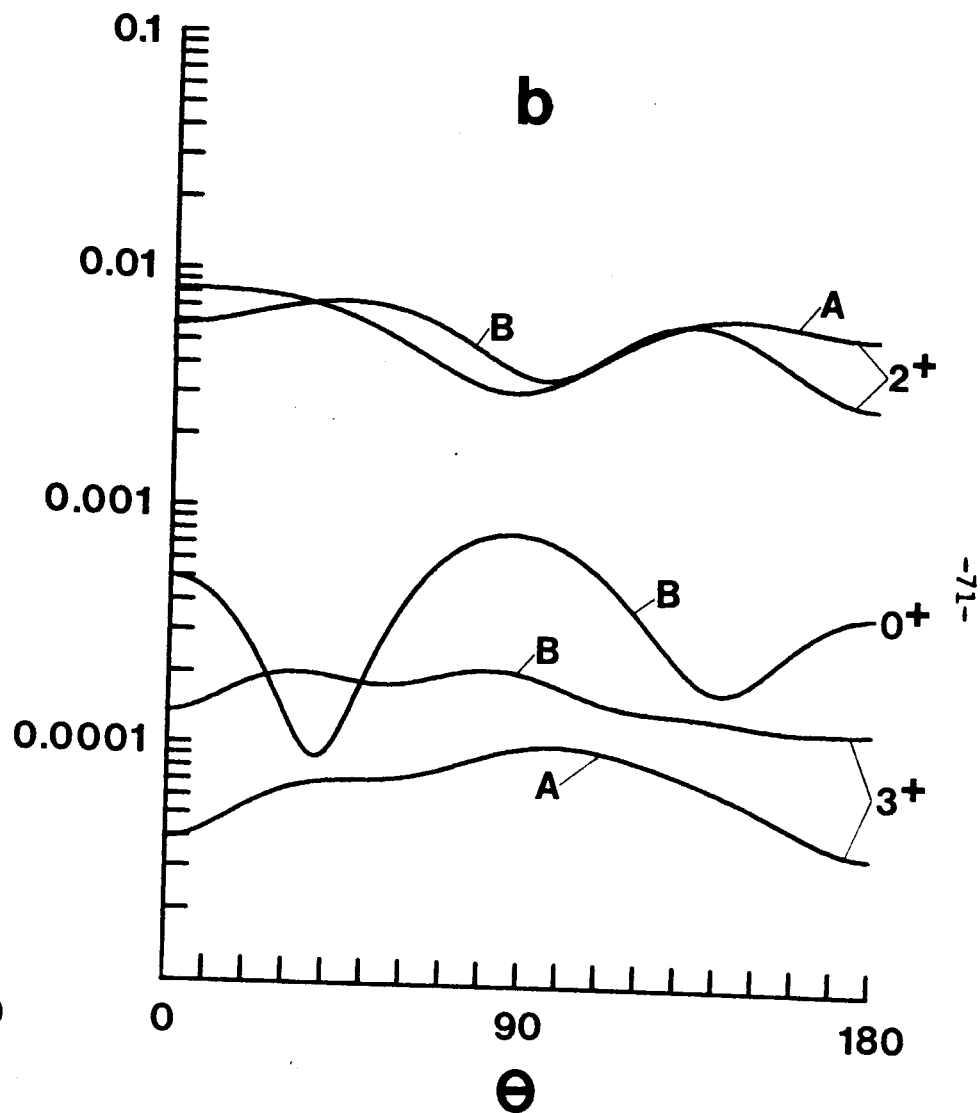
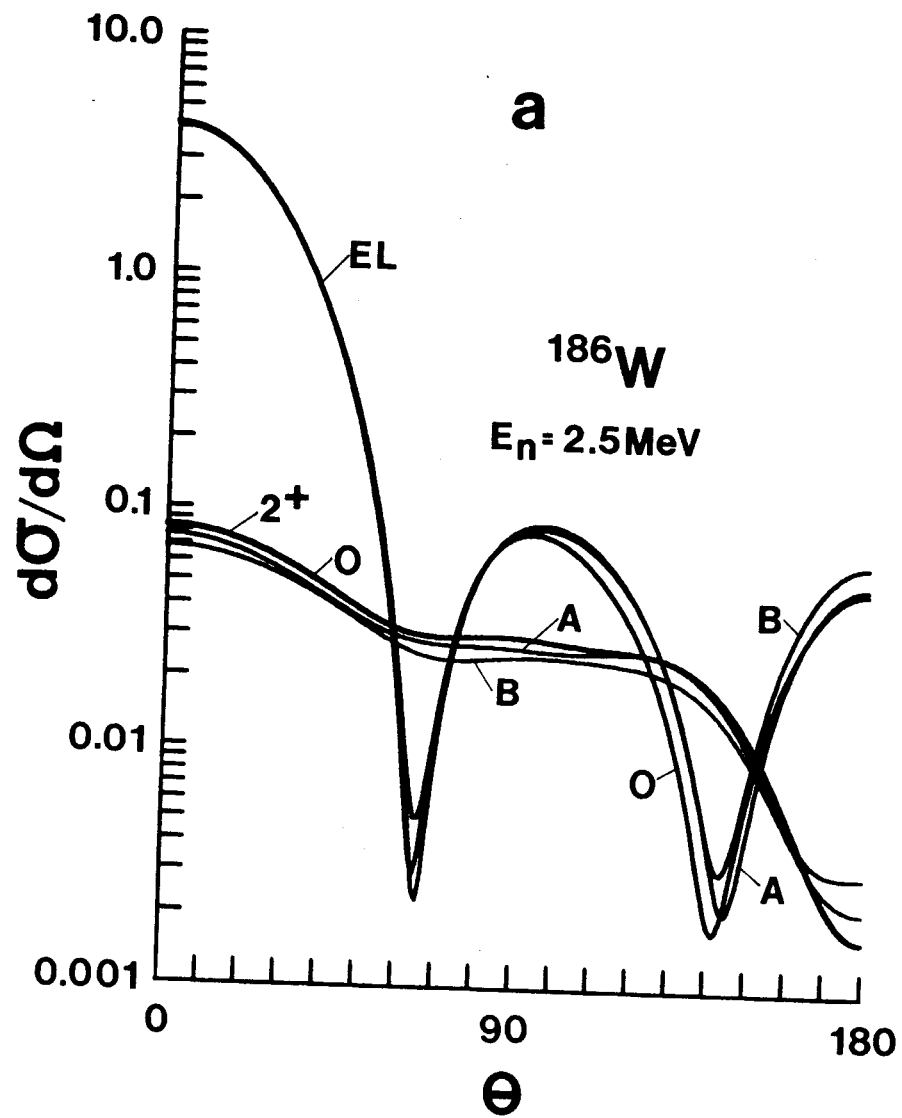


Fig. IV-14.

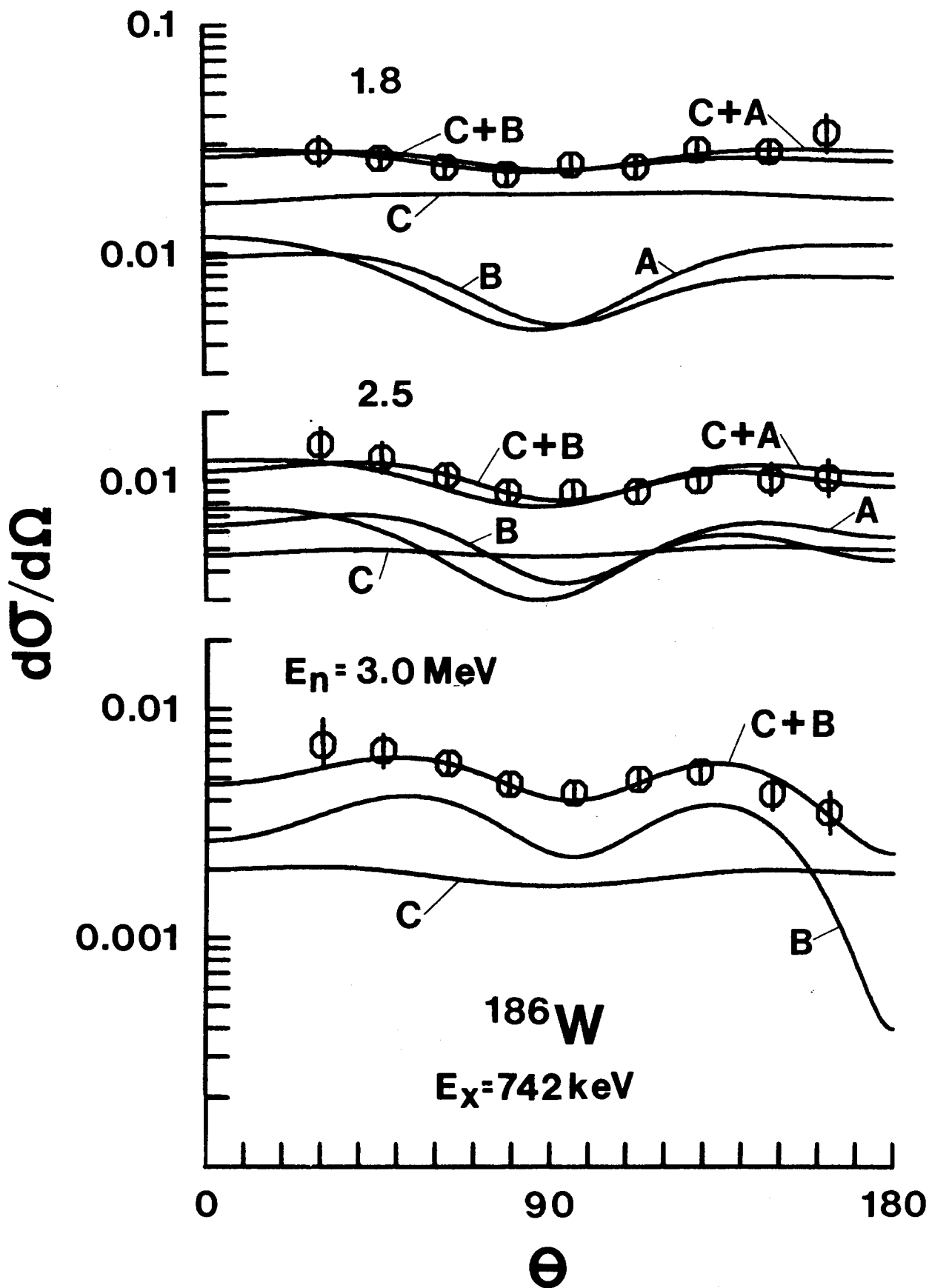


Fig. IV-15.

## V. EVALUATED NUCLEAR DATA FILE

This evaluation was primarily limited to neutron-interactions with the isotopes  $^{182}\text{W}$ ,  $^{184}\text{W}$  and  $^{186}\text{W}$  over the energy range of the present experiments and of those previously reported from this laboratory (V-1). The objective was the provision of a limited evaluation that can serve as an input to more comprehensive evaluation efforts to be reported elsewhere (V-2) and to provide a summary experimental data base for the comparisons of measured and calculated values as discussed in the previous section. The present measurements and those of Ref. V-1 provide a relatively comprehensive experimental basis for the evaluation excepting only radiative capture processes. For the latter, explicit reliance was placed upon the evaluation of Ref. V-3 and the experimental values cited therein. The numerical results of the present partial evaluations are given in Appendix A in the ENDF format (V-4).

### A. Neutron Total Cross Sections

The experimental data base is limited to four sets of results none of which span the entire energy range considered here (0.1-15.0 MeV). There is no experimental information above 15 MeV. Lister et al. (V-1) have reported detailed measurements over the range 0.1-0.65 MeV as the result of the application of monoenergetic-source techniques. These results were corrected for resonance self-shielding perturbations, as described in Sec. III, and averaged over a 20 keV resolution function so as to smooth the evident structure while at the same time retaining the character of the intermediate fluctuations. The present work provides detailed experimental results over the range 0.2-5.0 MeV. Martin et al. (V-5) have reported values over the range 0.7-15.0 MeV obtained using white-source techniques. Foster and Glasgow (V-6) have used similar methods to obtain detailed results over the range 2.3-15.0 MeV. The latter two white-source measurements were made over energy regions where the cross sections are expected to be energy-smooth therefore the data of each set was averaged over a 100 keV resolution function in order to remove fluctuations of an experimental origin. The four sets of data are not entirely consistent and therefore evaluation judgments were made as per the following.

In the case of  $^{182}\text{W}$  the results of Lister et al. provide the most detailed information in the low-energy region and they are supported by the results of the present work. The two sets of data are consistent to well within the respective experimental uncertainties considering the structure evident in the better-resolution work of Ref. V-1. Thus the evaluation relies primarily upon the results of Lister et al. to energies of 0.65 MeV. From 0.7 to 2.3 MeV two sets of experimental data are available; the results of Martin et al. and those from the present work. The two sets of results are similar in this energy range but the values of Ref. V-5 show systematic problems in the context of the other two isotopes that are a concern; therefore the evaluation relied upon the present work over the range 0.65-2.3 MeV. From 2.3 to 5.0 MeV the present results and those of Foster and Glasgow are essentially identical and both sets of values are somewhat larger than those reported by Martin et al. The evaluation in the 2.3-5.0 MeV range is constructed through an average of the results of the present work and those reported by Foster

and Glasgow. Above 5.0 MeV there are only two sets of experimental data available; those reported by Foster and Glasgow and by Martin et al. They are reasonably consistent but the latter is subject to much larger statistical uncertainties and thus the evaluation over the range 5.0-15.0 MeV relied upon the Foster and Glasgow results. The various aspects of the experimental data bases and a comparison of the measured and evaluated neutron total cross sections are illustrated in Figs. V-1 and -2.

The evaluation of the neutron total cross sections of  $^{184}\text{W}$  followed essentially the same rationale as outlined above for the  $^{182}\text{W}$  case. However, in this case the values of Martin et al. are very clearly discrepant with those obtained in the present work at low energies and inconsistent with an energy extrapolation of the results of Lister et al. Moreover, the results of Ref. V-5 are not consistent with the model interpretations discussed in Sec. IV, above. Therefore, the  $^{184}\text{W}$  results of Martin et al. were entirely abandoned. The data base and the evaluation are compared in Figs. V-1 and -2.

The evaluation procedure used for the neutron total cross sections of  $^{186}\text{W}$  was identical to that employed in the  $^{184}\text{W}$  case. Again, the values of Martin et al. appear seriously discrepant at lower energies and thus were abandoned. The evaluation and data base are compared in Figs. V-1 and -2.

With the limited experimental information available for the evaluation of the neutron total cross sections uncertainty estimates must be subjective. Guidelines setting forth such uncertainty estimates are given in Table V-1.

The present evaluations can be tested by constructing an "elemental" cross section from the appropriate isotopically-weighted average of the  $^{182}\text{W}$ ,  $^{184}\text{W}$  and  $^{186}\text{W}$  evaluations and comparing the result with the reported elemental neutron total cross sections of tungsten (V-7). The constructed "elemental" cross section represents  $\approx 85\%$  of the naturally occurring isotopes and it is unlikely that the total cross sections of the remaining  $\approx 15\%$  of the isotopes greatly differ from those of the three even isotopes studied here. The constructed "elemental" cross sections and the true measured values are consistent to within the respective experimental uncertainties.

## B. Elastic-neutron-scattering Cross Sections

The available experimental-neutron-elastic-scattering information was assembled into three isotopic data bases. Measured data was accepted only when relevant to the particular isotope and when the measurements reasonably resolved the elastic component from all inelastic contributions. With these criteria the available information was limited to energies of  $\lesssim 4.0$  MeV. Below energies of  $\sim 1.5$  MeV the only experimental information appears to be from the work of Lister et al. (V-1). These results are detailed and were obtained with good resolution over the energy range  $\lesssim 0.3$ -1.2 MeV. Approximately 200 keV averages of this data set were used in the evaluation. Above  $\approx 1.2$  MeV the experimental coverage was limited and the experimental resolutions less satisfactory, thus the results of Ref. V-1 were used only to 1.2 MeV. From 1.5 to 4.0 MeV there is a large body of experimental information as the

result of the present work which covers the energy-angle range in considerable detail. A third set of data was available at 3.4 MeV as reported by Delaroche et al. (V-8 and -9). The three sets of data are reasonably consistent as illustrated by the comparisons of Sec. III, above. The composite experimental data base for each isotope was least-square fitted with Legendre-polynomial series. The resulting polynomial coefficients were then fitted with smoothly-varying energy dependent curves and the evaluated quantities taken from the respective curves. In doing so most attention was given to low-order coefficients which are of most applied importance. The high-order coefficients were less well defined by the experiments but the consequent uncertainties primarily effected the details of the distributions (e.g. the exact character of the diffraction minima) which generally are not of applied significance. Uncertainty guidelines for the low-order (e.g.  $\leq 6$ ) terms are 5-10% and somewhat larger for the high-order terms, as estimated from the consistency of results obtained from the various experiments.

Inherent in the above evaluation process is the derivation of the angle-integrated elastic-scattering cross sections. These were believed known to 5-8%, again, judging from the consistency of measured and evaluated results. The angle-integrated elastic-scattering results were used for the deduction of the non-elastic cross sections. At energies  $\gtrsim 3.0$  MeV the partial cross sections were not completely resolved in any of the experiments and consequently there remains a continuum inelastic component that was dictated by the above non-elastic cross sections. Below  $\approx 3.0$  MeV the deduced non-elastic cross sections served as a verification check of the observed partial cross sections. In detail, the evaluated elastic-scattering cross sections were derived as the difference between the neutron total cross sections and the sum of the non-elastic partial cross sections in order to assure the mandatory internal file consistency. In doing so care was taken to assure that the elastic cross sections so derived were consistent with those independently deduced from the elastic-scattering measurements. In all cases Wick's Limit was adhered to (V-10). The relative elastic scattering angular distributions were finally expressed as  $f_l$  coefficients (V-4). The resulting evaluated differential-elastic-scattering cross sections are summarized in Fig. V-3. They are reasonably consistent with the model interpretations of Sec. IV, above. The deviation of the evaluated quantities from the calculated values is largest at the very extreme minima of the distributions where the evaluated cross sections are not as small as those calculated from the model. Such differences are of little, if any, applied importance. There is some fluctuation with energy in the evaluated distributions reflecting similar behaviors of the underlying experimental data bases.

### C. Neutron Inelastic-scattering Cross Sections

There are only three relevant inelastic-scattering experimental-data sets: 1) that of Ref. V-1 ( $\sim 0.3$ -1.5 MeV), 2) that of the present work (1.5-4.0 MeV), and 3) results for the excitation of the ground-state rotational band at an incident energy of 3.4 MeV from Refs. V-8 and -9. These three sets of data are outlined and compared in Sec. III, above. The present evaluations assumed the level energies of Ref. V-11 to excitations of  $\sim 1.0$  MeV. The energies of "levels" at excitations  $\gtrsim 1.0$  MeV were taken from the present measurements as summarized in Tables III-1A, B

and C. As evident in Fig. III-8, these "levels" are generally composites of contributions from a number of true levels far too closely spaced to be experimentally resolved and representing a level density far exceeding the capacity of the ENDF format. Truncation to the observed "levels" is generally not a limitation in most file applications. The evaluated neutron-inelastic-scattering cross sections were primarily deduced from the observed quantities supported by the results of the model calculations of Sec. IV, particularly near thresholds where experimental information is not available. Generally, the evaluations followed the "eyeguides" of Figs. III-12A, B and C and the calculated results of Figs. IV-8, 9 and 10.

The estimated uncertainties associated with the discrete-inelastic-excitation cross sections vary from 5-10% in the prominent and better-known cases (e.g. the excitation of the 2+ and 4+ levels of the ground-state rotational band) to considerably larger values for cross sections due to levels at much higher excitation energies. Many of the latter components are very speculative but the overall trend is reasonably known. As a consequence the total inelastic cross sections were believed known to ~10% to incident energies of 2.5-3.0 MeV. This conclusion was supported by the consistency of non-elastic cross sections as deduced from total and elastic-scattering cross sections and as obtained by summing non-elastic partial-cross-section components. Furthermore, a broad-group energy-transfer matrix derived from the discrete inelastic components will have reasonably accurate elements not particularly sensitive to contributions from a single observed "level". Thus the presentation has the merit of reasonably representing the observed inelastic excitation cross sections for most applications in a transitional region not well described by simple statistical prescriptions. The overall character of the discrete inelastic evaluations and their cumulative effect leading to the total inelastic-scattering cross sections are illustrated in Fig. V-4.

Neutrons resulting from the excitation of discrete levels were generally assumed to be isotropically distributed as indicated by observation (e.g. see Fig. III-13). An exception was the excitation of the first two levels of the ground-state rotational band (see Figs. III-9 and -10). In these two cases the evaluations included an anisotropy derived from observation and the model of Sec. IV. At low-energies the anisotropy associated with these two levels is small. At higher energies it can be large but there the energy transfer is relatively small and thus the exact character of the distributions is of minor applied importance.

Level-energies above  $\approx 3.0$  MeV levels were no longer observed and thus the sum of discrete-inelastic cross sections falls short of the total inelastic cross section and a continuum component is employed in the evaluations. In  $^{184}\text{W}$ , comparisons of total, elastic and non-elastic cross sections suggests that the continuum starts very near 3.0 MeV. Its magnitude is set by the differences between the observed cross sections as outlined in Sec. V-B, above. Similar comparisons for  $^{182}\text{W}$  suggested that the discrete-excitation cross sections for "levels"  $> 2.5$  MeV, as given by the eye-guides of Figs. III-12A, are too large by 10-15%. Such a discrepancy is well within the experimental uncertainty in this speculative region therefore the magnitudes of the  $^{182}\text{W}$  eye-guides in this region were correspondingly reduced before incorporating

them in the evaluation. An analogous problem was encountered in a similar energy region in the case of  $^{186}\text{W}$  only here the non-elastic cross section suggests that the eye-guides of Fig. III-12C underestimates the discrete inelastic magnitudes by  $\sim 10\%$  between  $\sim 2.5$ - $3.0$  MeV. This discrepancy was resolved by introducing the  $^{186}\text{W}$  continuum component at somewhat lower energies (i.e.  $\sim 2.5$  rather than  $3.0$  MeV). The fact that these small discrepancies are somewhat different in character for  $^{182}\text{W}$  and  $^{186}\text{W}$  may reflect differences in the underlying level structure in the context of the experimental resolutions. The general nature of these continuum components and the agreement between measured and evaluated elastic-scattering cross sections is illustrated in Fig. V-4. The evaluations assume that the continuum neutron emission is isotropically distributed. The corresponding energy-spectrum distributions are not given in the evaluations. It is reasonable to accept in this energy region one of the conventional statistical distributions, e.g. that of Gilbert and Cameron (V-12).

#### D. An Illustrative Comparison with ENDF/B-V

Portions of the present evaluation were compared with relevant sections of ENDF/B-V (V-4).  $^{186}\text{W}$  was arbitrarily selected for this purpose for the pragmatic reason that the corresponding ENDF/B-V isotopic file was readily available. Some of these comparisons are illustrated in Fig. V-5. There are large differences between the present evaluation and that of ENDF/B-V. Neutron total cross sections can differ by  $\pm 5$ - $10\%$  in magnitude. In some energy regions neutron elastic-scattering cross sections are discrepant by  $15$ - $20\%$  and differences in the neutron total inelastic-scattering cross sections can be  $10\%$  or more. In addition, the present representation of neutron inelastic-scattering is very different from that of ENDF/B-V with the latter giving far more emphasis to the continuum-inelastic component. These are large differences in both magnitude and character that make more detailed comparisons of questionable value.

References, Section V.

- V-1. D. Lister, A. Smith and C. Dunford, Phys. Rev., 162 1077(1967); see also J. F. Whalen et al., Argonne Natl. Lab. Report, ANL-7210 (1966).
- V-2. E. Arthur et al., to be published (1981).
- V-3. G. Grenier, J. Delaroche, S. Joly, Ch. Lagrange and J. Voignier, Neut. capture cross sections of Y, Nb, Gd, W and Au between 0.5 and 3.0 MeV, Proc. Conf. on Nucl. Cross Sections for Technology, Natl. Bureau of Stds. Pub., NBS-SP-594 (1980).
- V-4. Brookhaven Natl. Lab. Report, ENDF-102, 2nd edition, Editor R. Kinsey (1979).
- V-5. R. C. Martin, P. F. Yergin, R. H. Augustson, N. N. Kaushal, H. A. Medicus and E. J. Winhold, Bull. Am. Phys. Soc., 12, 106(1967).
- V-6. D. Foster and D. Glasgow, Phys. Rev., C3 576(1971).
- V-7. Brookhaven Natl. Lab. Report, BNL-325, Vol.-II, 3rd edition, Editors D. Garber and R. Kinsey (1976).
- V-8. J. Delaroche, G. Haouat, R. Shamu, J. Lachkar, M. Patin, J. Sigaud and J. Chardine, Proc. of Natl. Soviet Conf. on Neutron Physics, Kiev (1977); Also to be published in the Phys. Rev.
- V-9. J. Lachkar et al., Proc. of Inter. Conf. on Nuclear Data for Reactors and other Applications, Harwell (1978).
- V-10. See R. Lane and R. Thomas, Revs. of Mod. Phys., 30 257(1958).
- V-11. Table of Isotopes, 7th edition, Editors C. M. Lederer and V. S. Shirley, Wiley Interscience Pub., New York (1978).
- V-12. A. Gilbert and A. Cameron, Can. Jour. Phys., 43 1446(1965).

Table V-1. Total-cross-section Uncertainty Guidelines<sup>a</sup>

$E_n$ (MeV)	$\pm$ Uncertainty (%)	$E_n$ (MeV)	$\pm$ Uncertainty (%)
0.1	3.0	5.0	2.0
0.5	2.0	6.0	2.0
1.0	1.5	8.0	3.0
2.0	1.5	10.0	3.5
3.0	1.5	14.0	5.0
4.0	1.5		

<sup>a</sup>Linear energy interpolations are approximately valid.

Figure Captions, Section V.

- Fig. V-1. Comparison of measured and evaluated neutron total cross sections of  $^{182}\text{W}$ ,  $^{184}\text{W}$  and  $^{186}\text{W}$  from 0.1 to 5.0 MeV. The present evaluation is indicated by a heavy curve and the present experimental results by circular data symbols. Averages of previously reported data are indicated by light curves noted as follows: "W" = 20 keV average of Ref. V-1, "M" = 100 keV average of Ref. V-5, and "F" = 100 keV average of Ref. V-6.
- Fig. V-2. Comparison of measured and evaluated neutron total cross sections of  $^{182}\text{W}$ ,  $^{184}\text{W}$  and  $^{186}\text{W}$  from 5.0 to 15.0 MeV. The present evaluation is indicated by the heavy curve. Averages of reported experimental results are indicated by light curves as follows: "M" = 100 keV average of Ref. V-5 and "F" = 100 keV average of Ref. V-6.
- Fig. V-3. Evaluated differential-elastic-scattering cross sections of  $^{182}\text{W}$ ,  $^{184}\text{W}$  and  $^{186}\text{W}$ . Cross sections are given in b/sr and scattering angle in lab.-deg.
- Fig. V-4. Outline of present evaluations for  $^{182}\text{W}$ ,  $^{184}\text{W}$  and  $^{186}\text{W}$ . Curves indicate the evaluated cross sections identified as follows: 1 = total, 2 = elastic, 4 = total inelastic, 102 = capture and 91 = continuum inelastic. The cumulative envelopes of the discrete-inelastic components are shown by curves. Data points indicate measured elastic-scattering values:  $<1.5$  MeV from Ref. V-1,  $\geq 1.5$  MeV from this work.
- Fig. V-5. Comparison of components of the present  $^{186}\text{W}$  evaluation with those of ENDF/B-V. The heavy curves are from ENDF/B-V and the light ones from the present evaluation. Numbers denote reaction types as follows: 1 = total cross sections, 2 = elastic cross sections, 4 = total inelastic cross sections, and 91 = continuum inelastic cross sections.

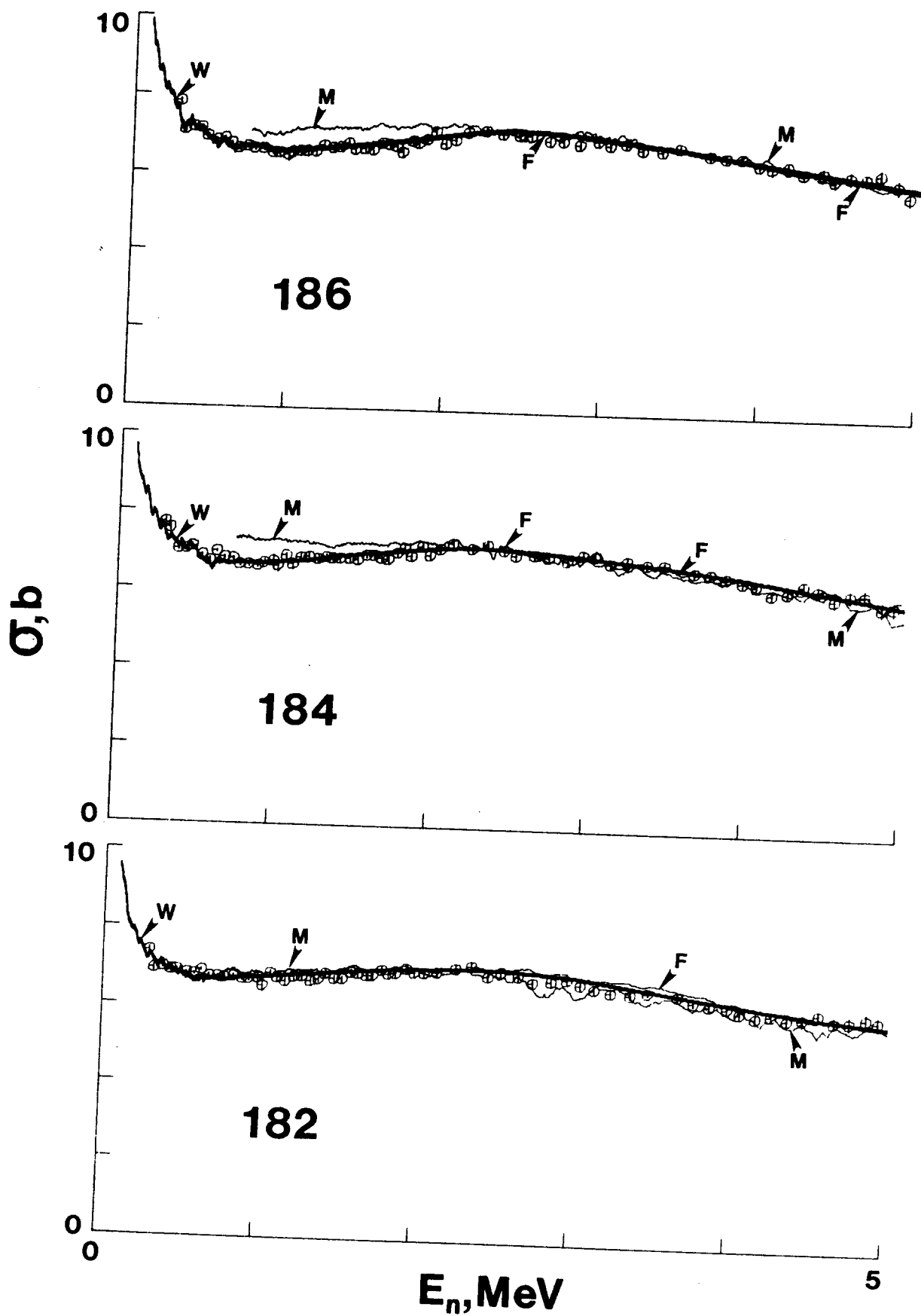


Fig. V-1.

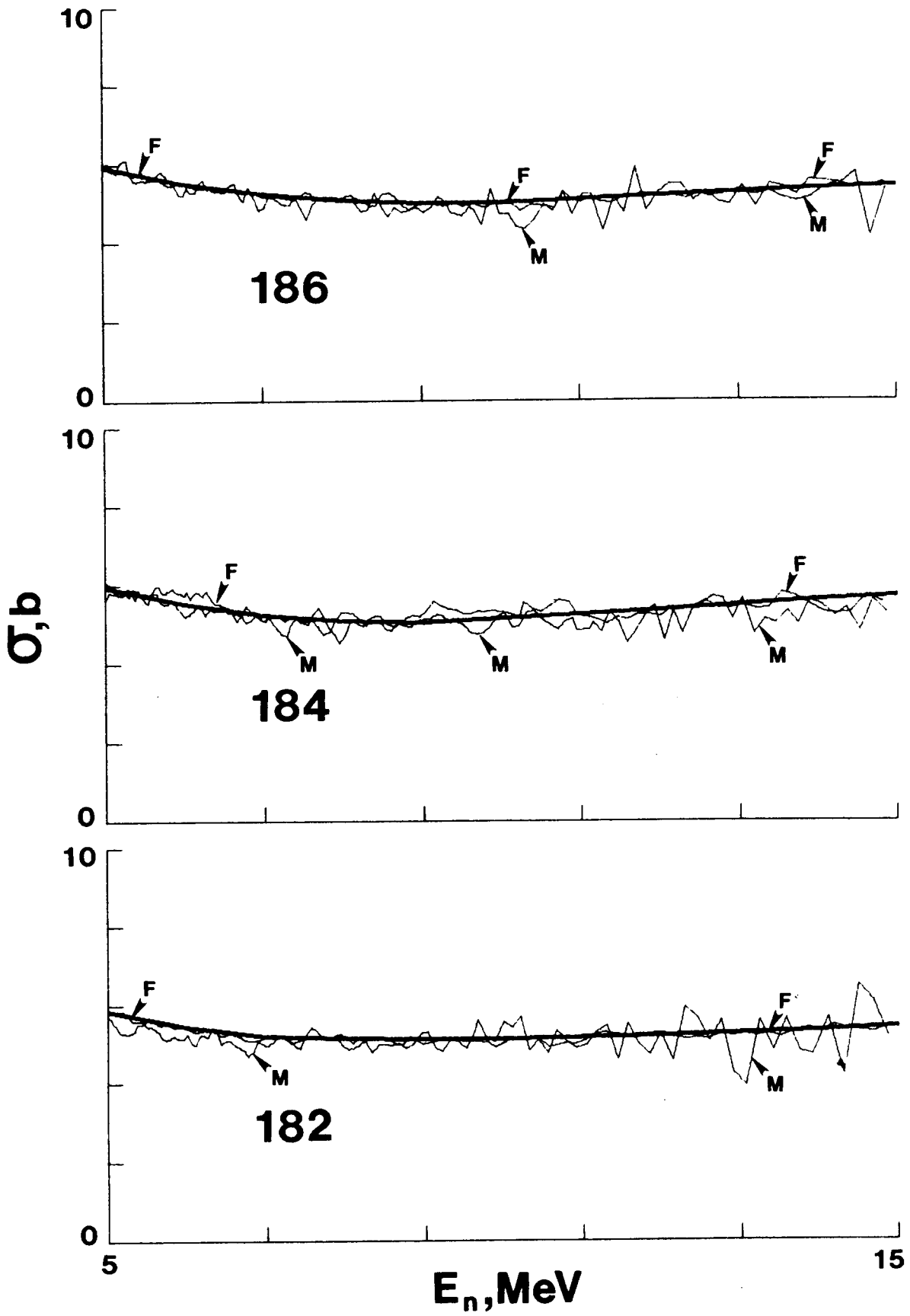


Fig. V-2.